

EFFECT OF DEGREE OF BIAXIALITY OF STRESS
ON THE RATE OF FATIGUE CRACK PROPAGATION

A Thesis Submitted

to

the Faculty of the Graduate Studies
The University of Manitoba

In Partial Fulfillment
of the Requirements for the Degree
Master of Science in Engineering (Mechanical)

by

Sunil R. Joshi

May 1969

c Sunil R. Joshi 1969



Acknowledgement

The author wishes to express his sincere thanks to Dr. John Shewchuk, Associate Professor and thesis advisor for his guidance and encouragement throughout the research program.

Thanks are also due to the technicians for their patience and help in constructing the experimental apparatus. Direct support received from National Research Council of Canada by means an operating grant is also gratefully acknowledged.

TABLE OF CONTENTS

	<u>Page</u>
Acknowledgements	ii
List of Tables	v
List of Figures	vi
Nomenclature	viii
Chapter 1. Introduction	1
1.1 Introduction	1
1.2 Statement of Problem	2
1.3 Scope of Thesis	2
Chapter 2. A review of Investigations Concerning Fatigue Crack Propagation	3
2.1 Introduction	3
2.2 The Mechanics of Crack Growth.	6
2.3 The Effect of Temperature	10
2.4 The Effect of Anisotropy.	12
2.5 The Effect of Variable Stress Fields	12
2.6 Fractography	21
2.7 Quantitative Approach to Crack Propagation	22
2.8 Summary	38
Chapter 3. Development of Biaxial Fatigue Crack Propagation Theory	39
3.1 Introduction	39
3.2 Uniaxial Fatigue Crack Propagation Theory	39
3.3 Octahedral Shear Stress Theory	42
3.4 Biaxial Fatigue Crack Propagation Theory	42
Chapter 4. Experimental Study	45
4.1 Introduction	45
4.2 Material and Specimens	45
4.3 Test Equipment.	49
1. Plate Testing Machine	49
2. Hydraulic Pressure Supply	57
4.4 Calibration and Measurements	58
4.5 Testing Procedure and Observations.	58
1. Procedure for Plate Testing	63

Table of Contents (Continued)

	<u>Page</u>
Chapter 5. Results and Discussion	64
5.1 Test Results	64
5.2 Analysis of Test Results.	64
1. Introduction	64
2. Determination of Constants	64
5.3 Discussion	73
Chapter 6. Summary and Conclusions	76
6.1 Summary	76
6.2 Conclusions	76
6.3 Suggestion for Further Study	77
Bibliography	78

LIST OF TABLES

<u>Table</u>		<u>Page</u>
4-1	Chemical Composition of 2024-T351 Aluminum Alloy .	46
4-2	Mechanical Properties of 2024-T351 Aluminum Alloy .	46
4-3	Description of Specimens	48
4-4	Testing Program	62
5-1A	Crack Length, l , at Different Number of Cycles for Specimens of Series A	67
5-1B	Crack Length, l , at Different Number of Cycles for Specimens of Series B	68
5-1C	Crack Length, l , at Different Number of Cycles for Specimens of Series C	69

LIST OF FIGURES

<u>Figure</u>		<u>Page</u>
2.1	The S-N Curve and the Cracking Line for SAE 1020 Steel	4
2.2	Effect of Surface Finish on the Growth of Cracks . . .	5
2.3	The Stress Distribution in the Vicinity of a Crack Tip.	7
2.4	The Two Stages of Crack Propagation	9
2.5	Various Types of Morphology Exhibited by Striations on Ductile Fatigue Fracture Surface	11
2.6	S-N Curve for Titanium Alloy at Different Temperature .	13
2.7	Growth of Fatigue Cracks as a Function of Temperature .	14
2.8	Anisotropic Flaw Growth	15
2.9	Growth of Crack as a Function of Types of Test Loading.	16
2.10	Typical Damage Accumulation for Laboratory Tests of Complex Structure	17
2.11	Delay in Crack Propagation for 2024-T3 Aluminum Alloy Under Two Step Tests	19
2.12	Comparison of Crack Propagation in Constant-Amplitude and High-Low Two-Step Tests for 2024-T3 Aluminum Alloy	20
2.13	Hypothesis on the Formation of Striations	23
2.14	Stress Intensity versus Cracking Rate	24
2.15	The Concept of Fracture Growth Under a Static Load .	26
2.16	The Concept of Fracture Growth Under Repeated Load .	28
2.17	Ratio of Length of Plastic Zone to Crack Length for Mild Steel	31
2.18	Schematic Diagram of a Section of an Axially Loaded Sheet Specimen	32
2.19	Correlation Between Crack Propagation Factor and Stress Range	35
4.1	Specimen Dimensions.	47

LIST OF FIGURES (Continued)

<u>Figure</u>		<u>Page</u>
4.2	Test Equipment.	50
4.3	Schematic Diagram of Testing Machine	51
4.4	Electrical System for Biaxial Fatigue Machine	52
4.5	Opening End of Pressure Chamber	53
4.6	Exploded View of Specimen Holder	55
4.7	Specimen Holder and Seals	56
4.8	Strain Gage Locations for Plate Specimens	59
4.9A	Instruments for Calibration	60
4.9B	Specimen with Strain Gauges	60
4.10	Stress Profile at Test Pressure for the Three Series of Specimens	61
5.1	Crack Length versus Number of Cycles for 2024-T351 Aluminum Alloy	65
5.2	Crack Length versus Number of Cycles for 2024-T351 Aluminum Alloy for Crack Length up to 1 inch	66
5.3	Typical Fracture Patterns	71
5.4	Rate of Crack Propagation versus Stress Intensity Factor for 2024-T351 Aluminum Alloy	72
5.5	Rate of Crack Propagation versus Stress Intensity Factor for 2024-T351 Aluminum Alloy Extrapolated up to Zero Rate of Crack Propagation	74

NOMENCLATURE

R	resistance to crack growth
G	crack driving force
l	crack length
a	half crack length
l'	effective crack length
d	size of plastic zone
N	number of cycles
t	thickness of plate
L	width of plate
η	number of cycles of stress for particular stage
K	stress intensity factor
K_N	effective stress concentration factor
r	rate of crack propagation
ρ_1	radius of crack tip
β	ratio of minimum to maximum stress
B_1	configuration of crack
B_2	complete stress-strain relationship
E	elastic modulus
σ_0	elastic stress
σ_Y	yield stress
σ_A	alternating stress
S_{NET}	actual sectional stress
S_e	endurance limit
σ_F	fracture strength

NOMENCLATURE (Continued)

τ_{oct} shear stress on the octahedral plane

S_f fatigue limit

τ'_{oct} octahedral fatigue limit

ΔS stress range

$C, A, A_1, \left. \begin{array}{l} \\ A_2, A_3, A_4, \end{array} \right\}$ material constants

CHAPTER 1

Introduction

1.1 Introduction

The rate of propagation of fatigue cracks is a subject not only of academic but also of practical interest as applied to multi-component design. Knowledge of the significant parameters affecting the rate of propagation of fatigue cracks is useful in application to designing.

Crack propagation is the only phase of fatigue failure which can be treated quantitatively without the added complication of statistical fluctuations. Moreover, in many materials, and especially in notched structures, the crack propagation phase occupies a major fraction of the useful life. There is, in fact one school of thought which views all of fatigue damage as the growth of cracks or cracks which grow from pre-existing flaws in real structures.

In recent years an enormous amount of effort has been devoted to the study of fatigue crack propagation. Careful microscopic or macroscopic observation of growing fatigue cracks has led to semi-quantitative models for the crack extension process. Finally, the results of crack propagation research are becoming useful tools which can be used in designing real structures.

A considerable amount of experimental and theoretical research has been conducted on fatigue crack propagation. However, as the literature survey will indicate, the bulk of this has been in the field of uniaxial stress and strain cycling. Since many machines and structural parts are subjected to combined fatigue stresses, it is desirable to understand the effect of biaxial stress on fatigue crack propagation.

1.2 Statement of Problem

This thesis is a theoretical and experimental study of the effect of degree of biaxial stress on the rate of fatigue crack propagation.

1.3 Scope of Thesis

The thesis is divided into six chapters.

Chapter 1 is an introduction to the field of fatigue crack propagation.

A review of existing material on fatigue crack propagation is presented in Chapter 2.

Chapter 3 presents a modification of the uniaxial fatigue crack propagation theory based on the octahedral shearing stress theory for application to biaxial stress conditions.

The experimental program which was carried out to check the validity of the proposed theory is described in Chapter 4.

Chapter 5 presents the test results and conclusions.

The thesis is summarised in Chapter 6.

A bibliography is presented at the conclusion of the thesis.

CHAPTER 2

A Review of Investigations Concerning Fatigue Crack Propagation

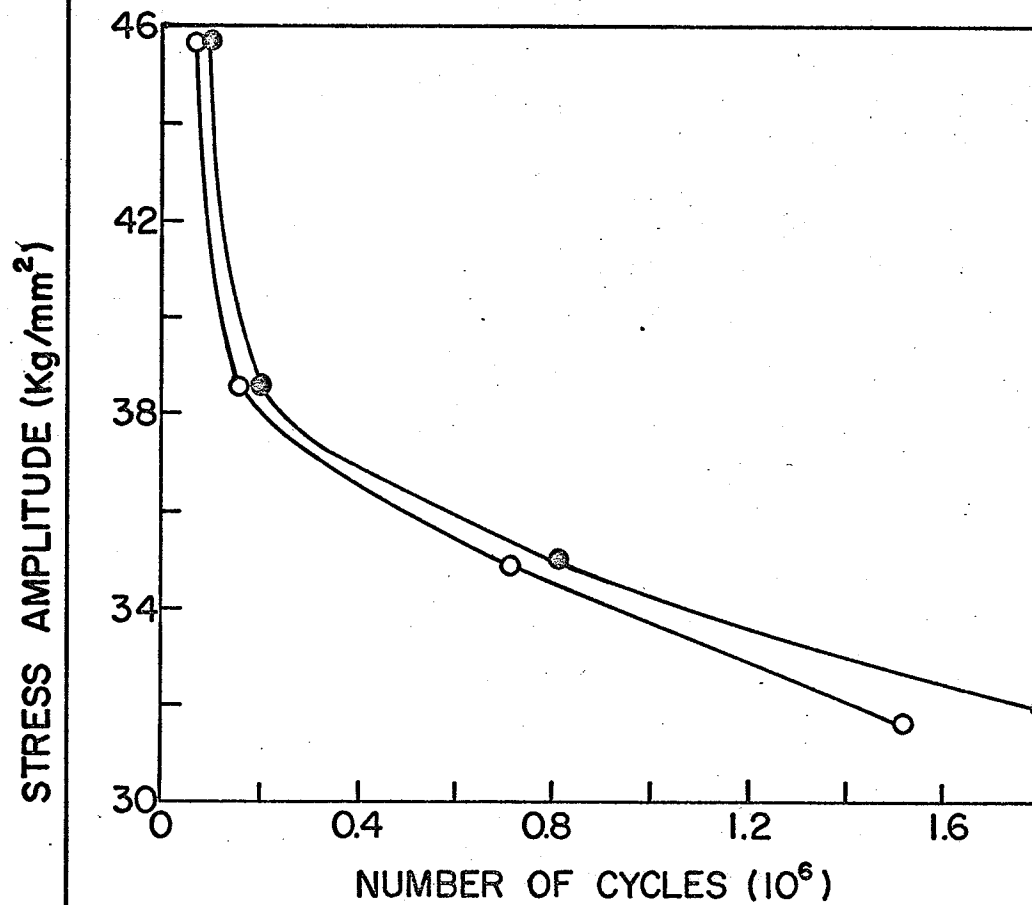
2.1 Introduction

The number of cycles required to produce final fracture or rupture subsequent to the first detection of cracks is governed directly by the rate of crack growth. This number is of great practical significance; if it is possible, for example, to predict that a certain crack will not induce a catastrophic fracture, then the use of the material for the components is sound. It is desirable, therefore, to discuss cracks in relation to the number of loading cycles and to seek characteristic behaviour at various stages of the fatigue process ranging from the state at which, by presently available means, cracks can first be detected to the advanced final phase of fracture.

Consider, first, several experimental results. When the stress amplitude is just above the endurance limit, microscopic cracks are found (Moore(1)) at about one half the fatigue life, but when the stress amplitude is somewhat greater than the endurance limit, they appear just prior to fracture, as shown in Figure 2.1. In small specimens, however, observable cracks have been initiated near the end of fatigue life, even though the stress amplitude was just above the endurance limit.

Forest (2) also observed the effect of stress on the rate of crack propagation by measuring the crack length as a function of number of cycles for specimens tested at different stress levels and different finishes, Figure 2.2.

Consider, finally, the formation of a crack in the root of a



SAE 1020 STEEL (AS COLD-ROLLED)
DIAMETER OF SPECIMEN = 16 mm

● = FRACTURE

○ = CRACK - DETECTION (CRACKS - 0.1 INCH LONG)

FIGURE 2.1 THE S-N CURVE AND THE CRACKING LINE

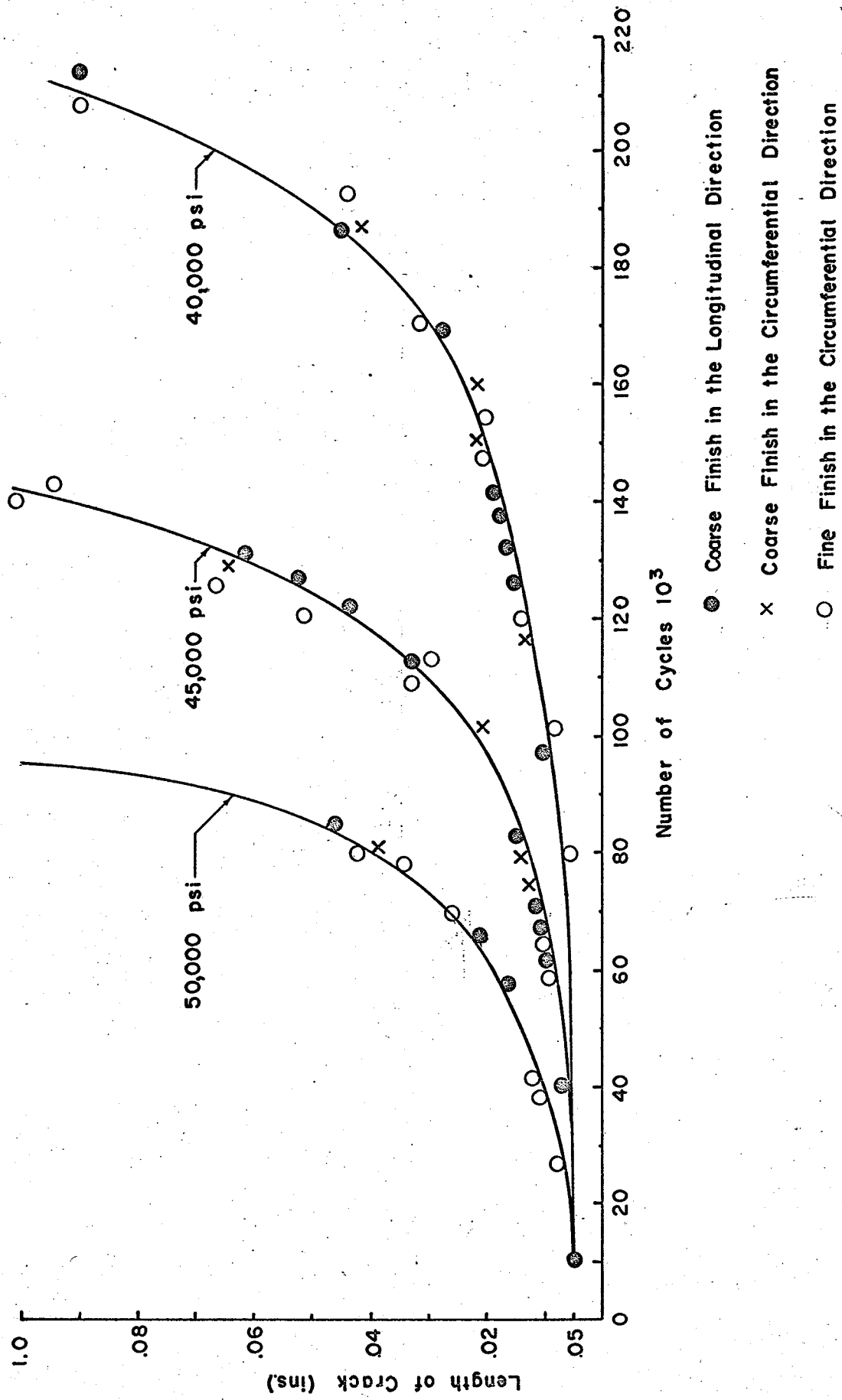


Figure 2.2 The Effect of Surface Finish on the Growth of Cracks

notch, which is the site of a high stress concentration or large stress gradient. There is ample experimental evidence that the growth rate is slow. This is true also of many practical situations in which a crack formed under high stresses, perhaps in manufacturing processes, is subjected to much smaller stress amplitudes in service. A large number of cycles are required to produce fracture even though cracks are initially present.

2.2 The Mechanics of Crack Growth.

It has been shown by many workers that the average direction of extension of a fatigue crack is generally perpendicular to the direction of maximum tension-compression. There are local deviations which are governed by the crystalline structure of the metal, but this factor will not be considered here.

Head (3,4) proposed a theory on the growth of a fatigue crack as follows: If the crack were in a purely elastic solid then applied loads would generate a high stress at the tip of the crack, as a result of the large stress concentration. In a metal this high stress would be above the yield stress and so a plastically deformed region would be created ahead of the tip of the crack. This has three consequences:

- a) As the plastic region yields, it work-hardens
- b) The plastic region is constrained by its elastic surroundings which, as yielding occurs, take up some of the load as shown in Figure 2.3, thus reducing the rate of stress increase in the plastic region.

- c) This increase in stress in the surrounding region will cause elastic region which originally carried a stress less than the yield

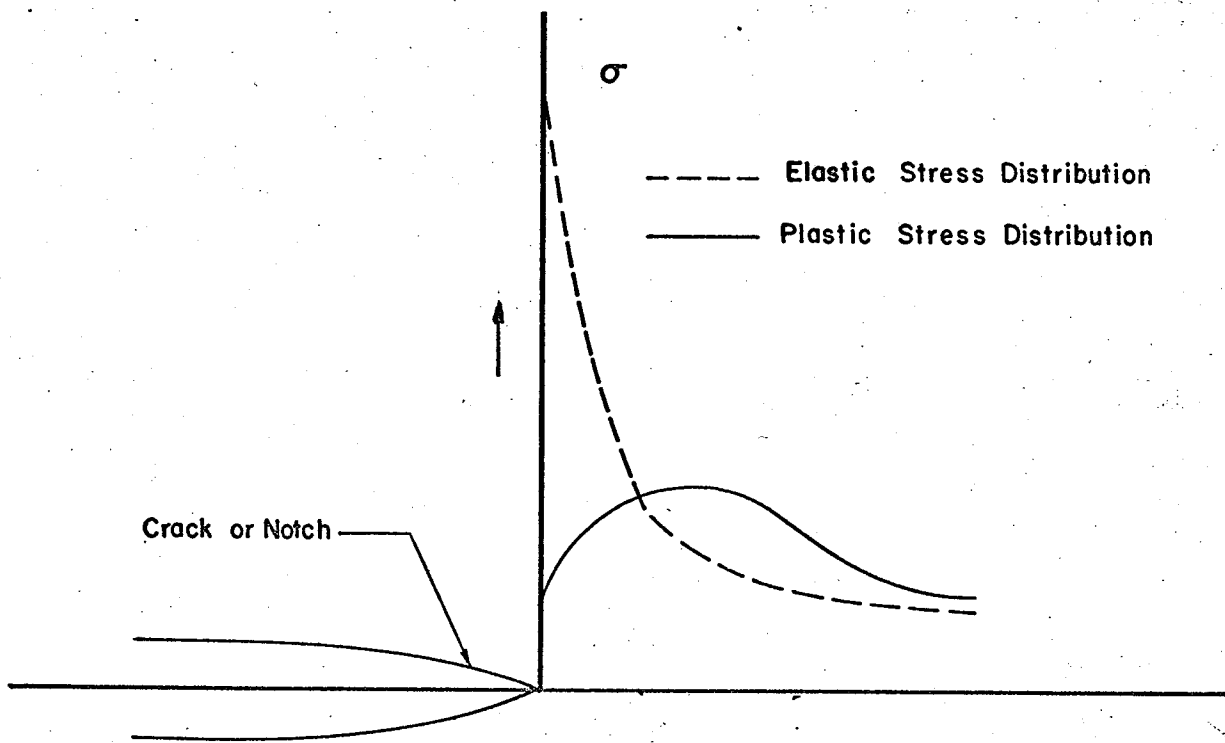


Figure 2.3 The Stress Distribution in the Vicinity of a Crack Tips [3]

stress, to be subjected to a large enough stress to become plastically deformed.

On reversing the applied stress, reverse plastic flow will occur, again governed by three effects mentioned. Continual application of an alternating stress will cause a continual work hardening at the tip of the crack, leading to one or the other of the following possibilities:

1. If the peak stress at the tip of crack in an elastic medium is less than the yield stress, then work-hardening will tend to a limit after which the applied stress causes elastic deformation only. In this case the crack does not spread.

2. If this peak stress under purely elastic deformation is greater than the fracture stress, then it is impossible for the material to work-harden sufficiently to produce a purely elastic state. Fracture in the neighbourhood of the tip of the crack will occur after a number of cycles. The crack then starts to spread with the same process being repeated at the new tip of the crack.

Consider the history of a small volume of metal in the line of advance of the crack. When the crack is far away the stress in the volume is essentially equal to the applied stress and the deformation is elastic. As the crack approaches, the stress rises, when it rises to the initial yield stress the volume becomes plastic and then describes a hysteresis loop, gradually work-hardening. When its ductility is gradually exhausted, it fractures and becomes part of the crack.

Campbell (5) suggested that crack propagation in fatigue takes place by two stages under a wide range of stressing and environmental conditions. The first stage, illustrated in Figure 2.4 is characterised

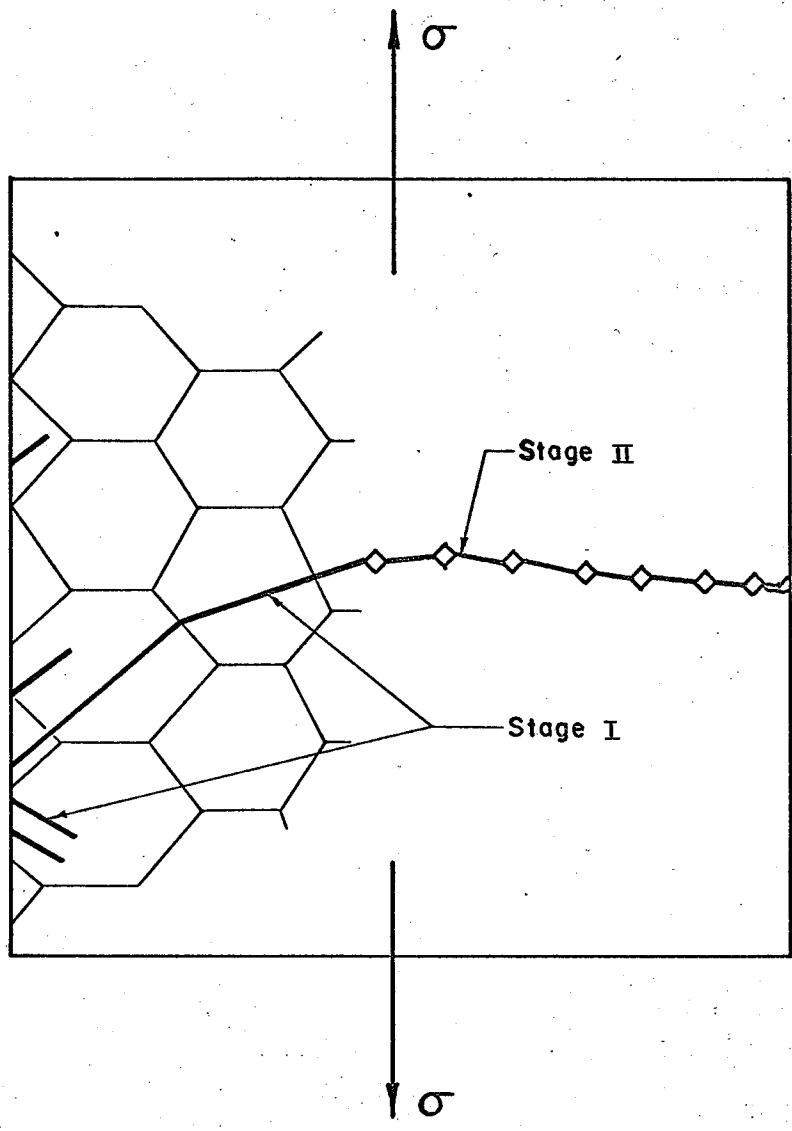


Figure 2.4 The Two Stages of Crack Propagation [5]

by propagation of the crack on a plane oriented at approximately 45° to the stress axis and by crystallographic fracture facets changing direction slightly with orientation at grain boundaries. Slight direction changes at grain boundaries are the rule, because the grains of most materials undergoing fatigue are not randomly oriented but textured by working and annealing processes. Subsequently, the propagation enters Stage II, also illustrated in Figure 2.4, where the plane of crack propagation is now at 90° to the stress axis and the fracture surface is covered by striations running parallel to the crack propagation front.

Since crack propagation rates in Stage II, can reach values of microns per cycle, the phenomenon associated with the growth mechanism are fairly large and relatively easy to observe. Most of the evidence for growth, therefore, concerns Stage II which has been proved to operate in the plastic blunting process. Figure 2.5 illustrates several types of profiles which have been observed in Stage II (6). Figure 2.5a is the one most commonly observed in ductile specimens broken at the highest stresses, and consists of parallel, juxtaposed depressions on both of the fracture surfaces. Fracture illustrated by Figure 2.5b occurs in the same circumstances as the first type. Ridges on one fracture surface fit depressions on the other. It is common, for a small crack, indicated by the arrowhead in Figure 2.5b, to undercut the ridges on the fracture surfaces. The types of striation shown in Figures 2.5c and 2.5d occur in specimens cycled at lower stress.

2.3 The Effect of Temperature

The effect of temperature on fatigue crack growth must also be considered: An example (7) is the S-N curve for a titanium alloy shown

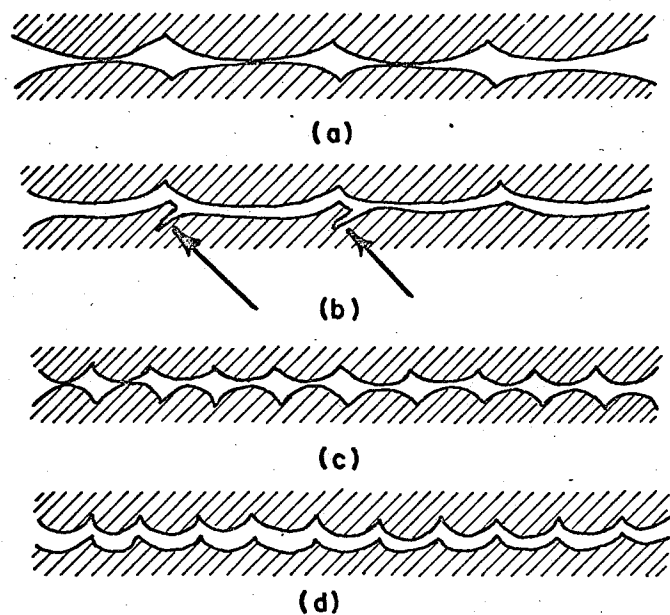


Figure 2.5 Various Types of Morphology Exhibited by Striations on Ductile Fatigue Fracture Surfaces [5]

in Figure 2.6. As would be expected, the fatigue life and physical properties degenerate as the temperature increases. It is of great interest to note that if laboratory data on the rate of crack propagation are plotted as a function of stress cycles and temperature, the result is a series of curves similar to those shown in Figure 2.7.

2.4 The Effect of Anisotropy.

The rate of propagation of a crack as a function of the cracks orientation with respect to the principal rolling direction of the commercial sheet used to build the sample is shown in Figure 2.8. The figure shows crack growth as a function of stress cycles for crack oriented at different directions with respect to the rolling direction of the sheet. (7). The basic mechanism of the phenomena of the fatigue crack growth as a function of the various crystallographic slip systems in the basic metal is not very well understood.

2.5 The Effect of Variable Stress Fields

Figure 2.9 shows a comparison of the crack growth as a function of stress cycles where: (1) the cyclic gross section stress or the maximum cyclic load is constant throughout the tests and (2) a constant cyclic net section stress is maintained by periodic reduction of test panel load. The crack growth rate is much higher for constant cyclic gross section stress.

Whaley and McGuigan M.J. (8) conducted tests on a large built-up wing structure, the actual test data is shown in Figure 2.10. The damage accumulation shown is typical of laboratory tests of complex structures. The curve has been normalized for three different tests

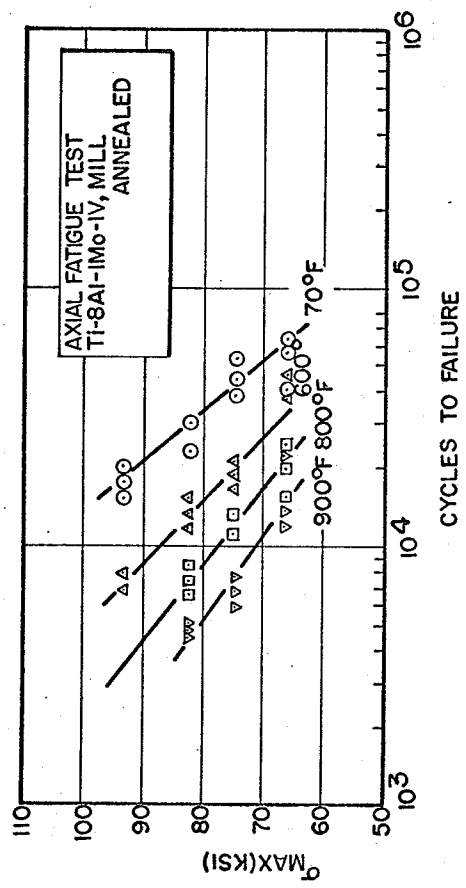


FIGURE 2.6 S-N CURVES FOR TITANIUM ALLOY AT DIFFERENT TEMPERATURES [7]

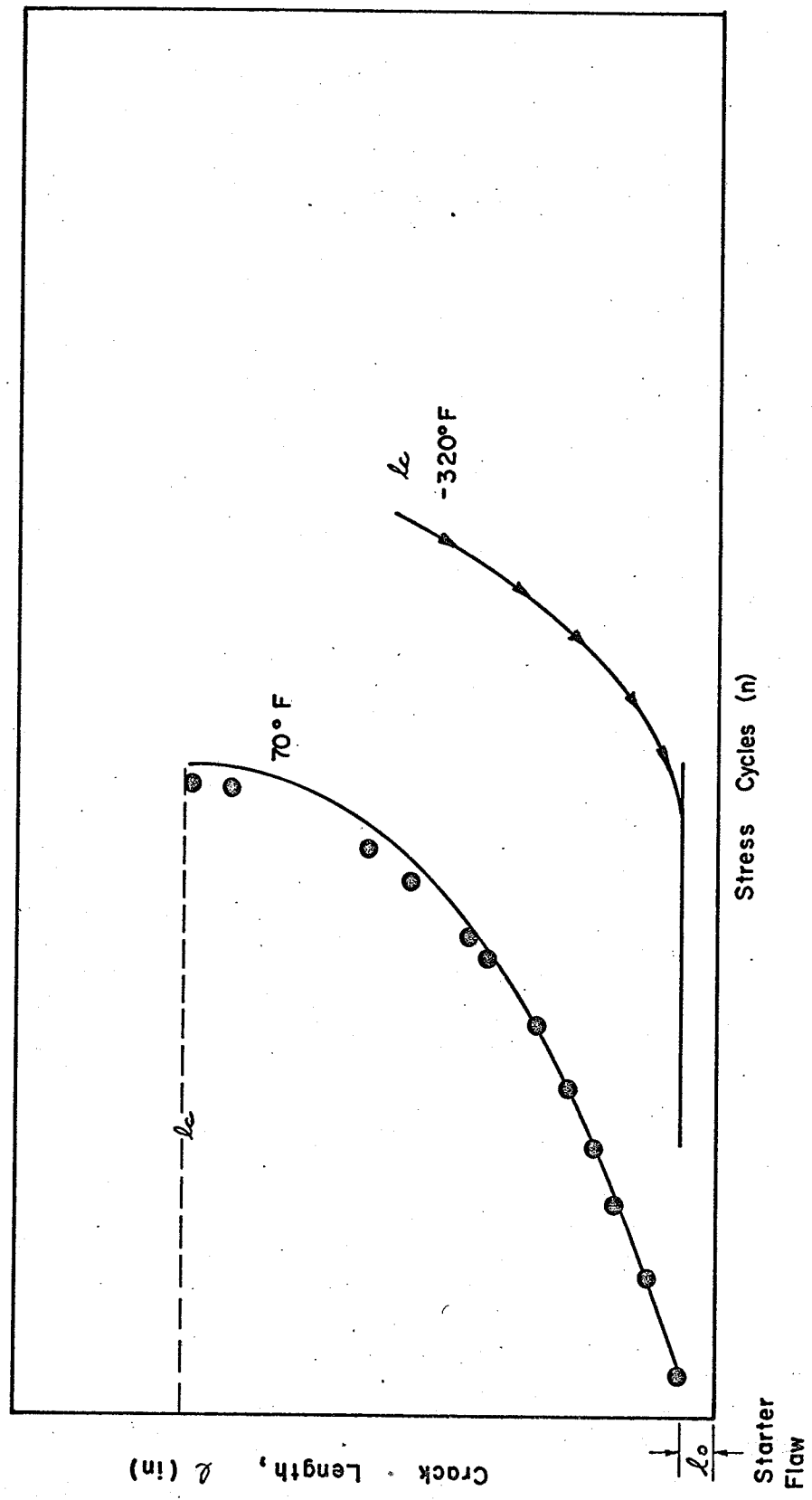


Figure 2.7 Growth of Fatigue Cracks as a Function of Temperature (Schematic)



Uniaxial Loading $\theta = 0^\circ =$ Angle of -
 $\sigma_y = \sigma_{max.} = 14,000$ -Rolling Dir.
 with Principal Load.

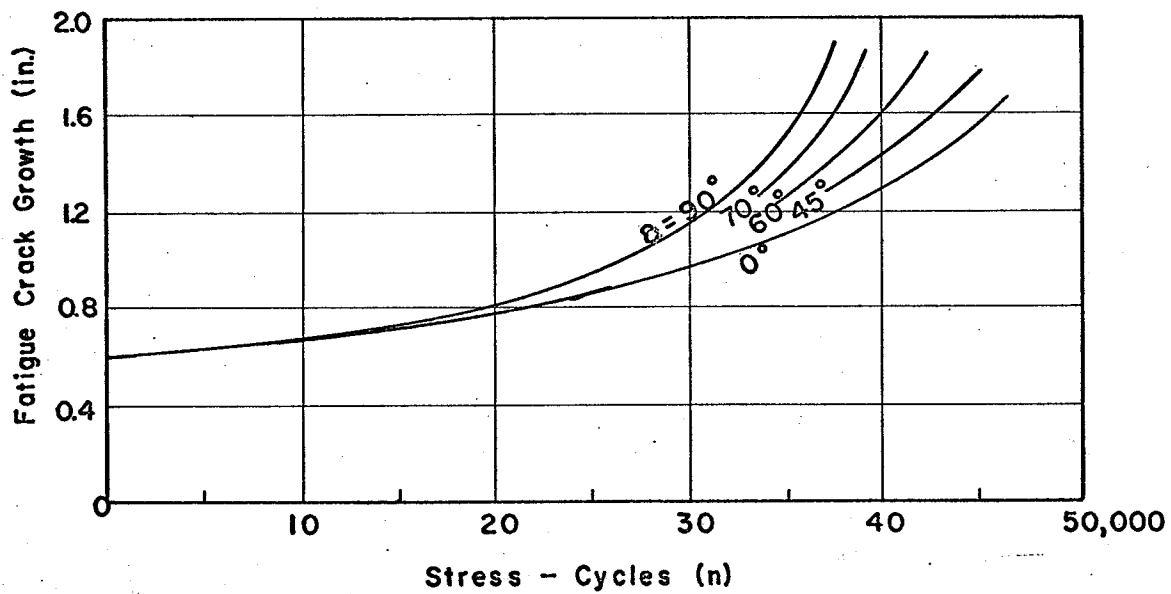


Figure 2-8 Anisotropic Flaw Growth [7]

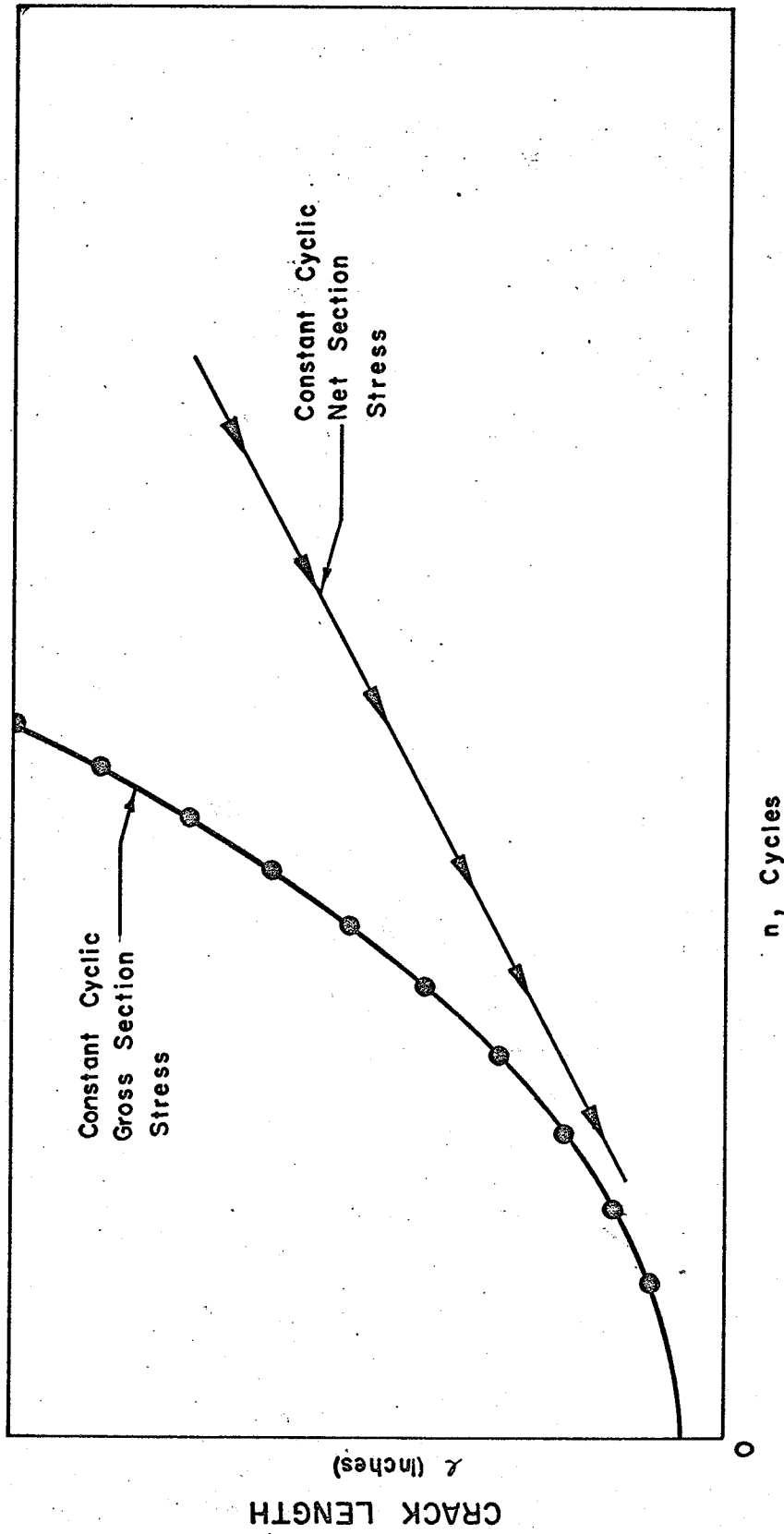


Figure 2.9 Growth of Crack as a Function of Type of Test Loading

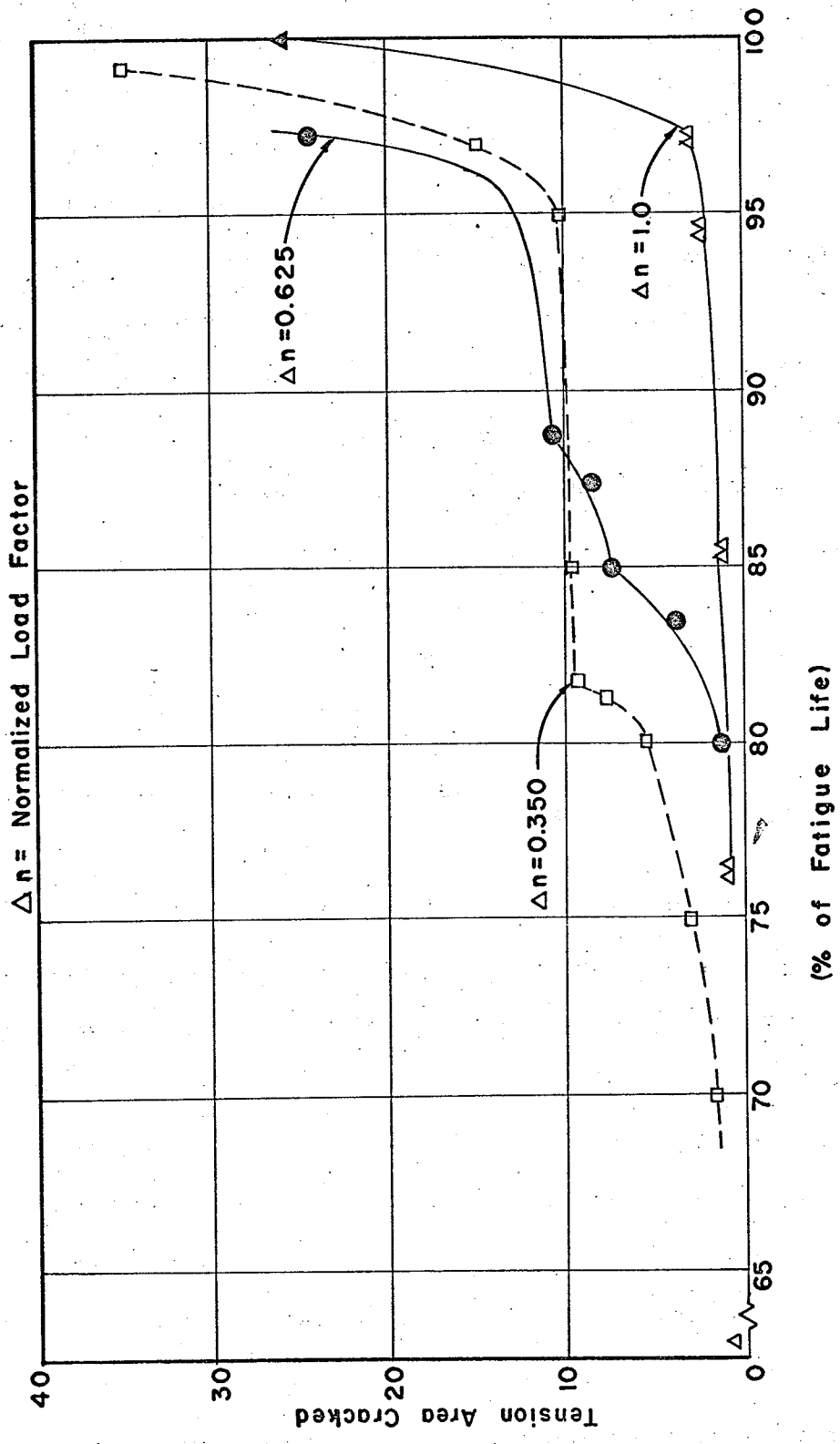


Figure 2.10 Typical Damage Accumulation for Laboratory Tests of Complex Structure

at three different stress levels.

Hudson (9) found that high load cycles succeeded by lower ones produced delays in fatigue crack propagation. Tests were conducted on 2024-T3 aluminum alloy specimens at two stress levels. Figure 2.11 shows that for a given second stress the higher the initial stress the greater the delay in crack propagation.

Hudson (9) performed some tests to determine whether previous loading history affected the rate of crack propagation once crack growth had again started at the second stress level. This determination was made by comparison of the number of cycles required to propagate the cracks for equal increments in the high-low two-step tests and in the constant amplitude tests. The interval over which this comparison was made began when the crack had propagated 0.1 inch past the crack length at which the stress levels were changed, and the interval extended to the point at which the specimens failed. This comparison is shown in Figure 2.12. The reference line shown on the figure is the locus of points along which the test points would lie if the rates of propagation in the constant-amplitude and the high-low two-step tests were the same. The generally close proximity of the test results to the reference line indicates that there is little difference between the rates of propagation in the constant-amplitude and two-step tests.

In the high-low test series, the lowest stress at which fatigue cracks would propagate to failure in 10^7 cycles was 16 ksi. This stress was considerably higher than the 10 ksi stress at which fatigue cracks were initiated and propagated to failure in constant-amplitude tests. Thus, it appears that the fatigue limit has increased. This result

Specimens of 2024 - T3 Aluminium Alloy

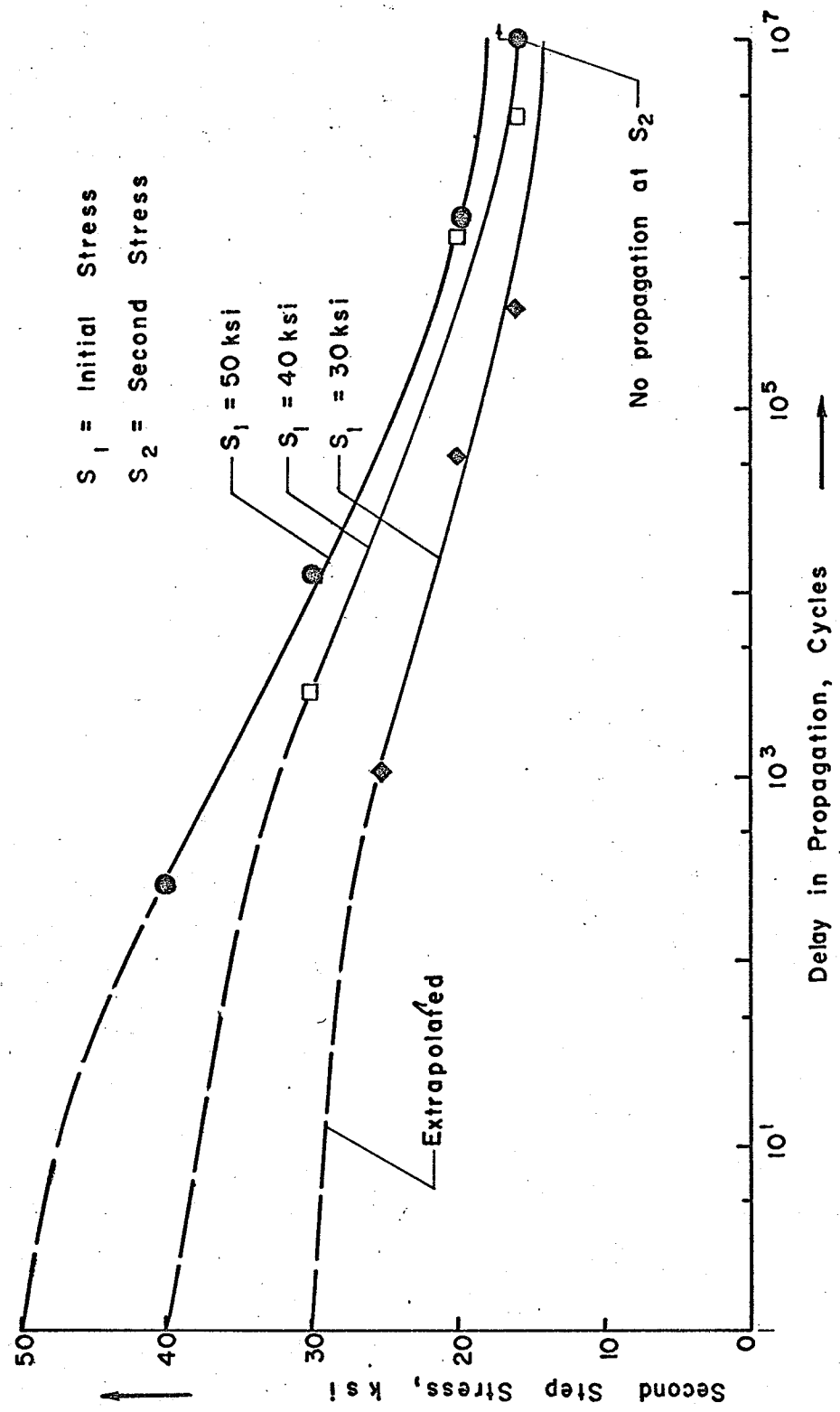


Figure 2-11 Delay in Crack Propagation

SPECIMEN OF 2024 T3 ALUMINUM ALLOY

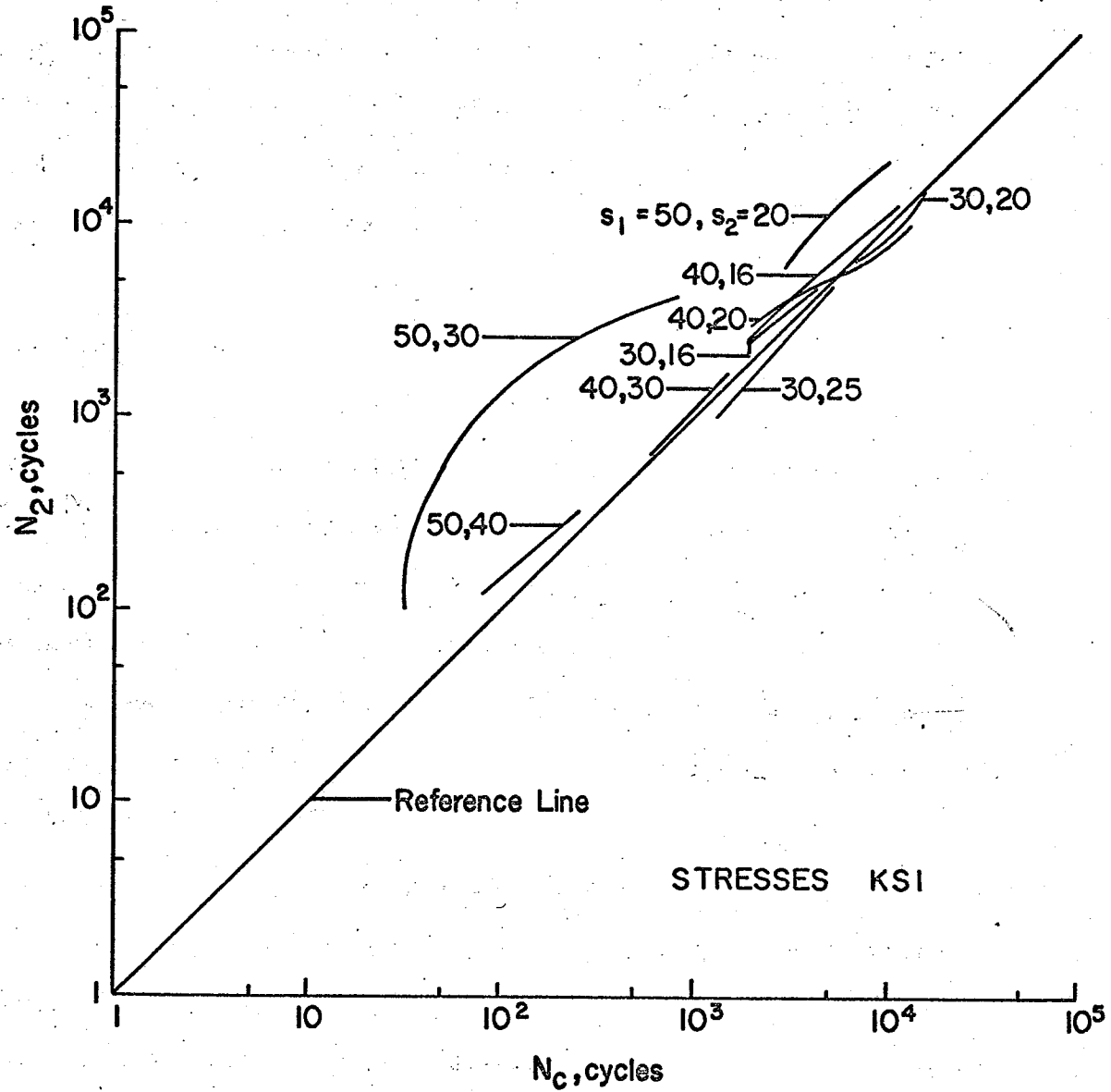


FIGURE 2.12 COMPARISON OF CRACK PROPAGATION IN CONSTANT-AMPLITUDE AND HIGH-LOW TWO-STEP TESTS

indicates that specimens subjected to variable-amplitude loadings may not be damaged by some stress cycles with magnitudes above the normal fatigue limit of the specimens.

These results help to explain why the linear cumulative-damage rule frequently produces erroneous estimations of the fatigue life of test specimens. This rule assumes that damage accumulates at a rate equal to the percentage of life used at a given stress level. Thus, this rule cannot predict the observed delay in crack propagation and the resultant increase in fatigue life.

2.6 Fractography

The use of electron microscopy for crack growth studies is increasing. Here the emphasis has been in the investigation of laboratory samples. Microfractography can only provide information about the crack growth stage (10) of the fatigue process and does not provide information on crack initiation mechanism.

The dominating feature of a fatigue fracture surface is a lamellar structure. Striations on a fracture surface should be considered as a typical feature of a fatigue fracture.

There are many hypotheses concerning the mechanism of striation formation. Laird and Smith (11) proposed that in a closed condition (zero load) the crack has a very small notch radius and, therefore, a very pronounced effect. With increasing load the radius increases and the crack "blunts" itself. At the same time as this plastic deformation, so-called "ears" occur in the direction of the theoretically derived maximum shear stresses. With return to zero load, a cavity remains in the crack tip area as a result of the "ears". Crack propagation is

resumed from the ears with the next load cycle, Figure 2.13. According to this hypothesis, which has been verified experimentally, the lines on fracture surfaces are depressions.

In the quantitative evaluation of crack propagation the principle is to count the striations from crack initiation up to final fracture and thus to determine the number of load cycles from initiation to rupture. If crack length is taken into account at the same time, the usual representation of crack propagation crack length as a function of the number of load cycles is obtained.

2.7 Quantitative Approach to Crack Propagation

It is well known that the phenomena of progressive fracture caused by fatigue can severely decrease the strength and life of a structure (7). Therefore, it is very important to collect and provide fatigue data in a form that is useful to designers.

Without exception, the fatigue crack equations available are valid only when applied within the limits of the particular test conditions.

Paris and Erdogan (12) attempted to normalize as much data as possible from different contributors. The method plots the crack growth rate per cycle as a function of stress intensity, which is proportional to the maximum cyclic stress and square root of the crack length as shown in Figure 2.14.

Cotterell (13) interpreted the cyclic growth as follows: There must be some relation between crack growth due to static load and that due to repeated loads.

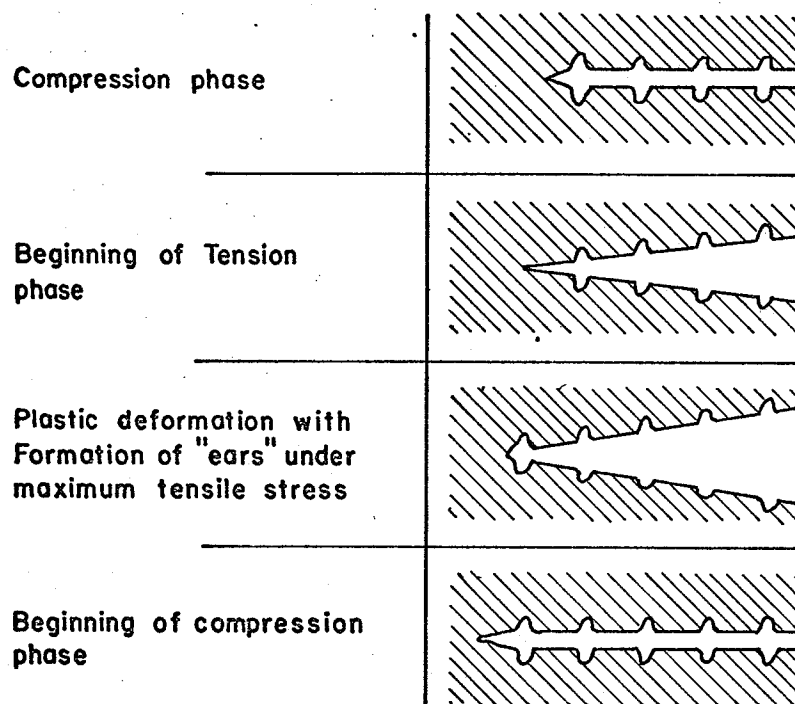


Figure 2.13 Hypothesis on the Formation of Striations

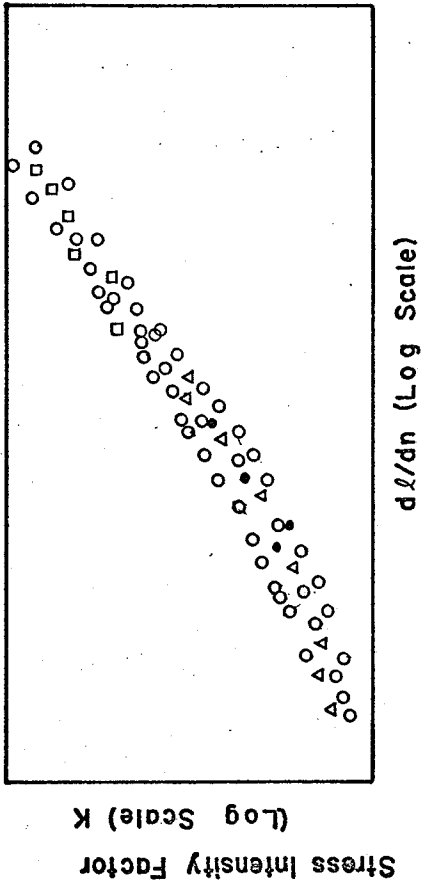


Figure 2-14 Stress Intensity versus Cracking Rate

He proposed:

$$G = \frac{\sigma_0^2 \pi l}{2E} \quad \dots 2.1$$

G = Crack Driving Force at the Tip of Crack

l = Crack length

σ_0 = Elastic Stress

E = Elastic Modulus

As the stress is increased, the available crack driving force can be represented in Figure 2.15 by a line of increasing slope. The resistance to crack growth, R , which is dependent only on absolute crack extension has a parabolic form. It is therefore possible for a crack to grow stably until the crack driving force G equals the resistance to crack growth, R . This crack growth will continue as the stress is increased, until the curve of crack driving force becomes a tangent to the crack resistance curve;

$$\text{i.e.,} \quad \frac{dG}{dl} = \frac{dR}{dl}$$

beyond this point, since now the crack driving force is always greater than the resistance to crack growth, the material becomes unstable and catastrophic failure occurs.

After a crack has been growing for a number of cycles there will be region of strain hardened material ahead of the crack. This strain hardening enables the crack to grow without gross deformation. It is reasonable to assume that the greater the strain hardening the easier it will be for the crack to grow. The strain hardening will be mainly dependent on the alternating stress, because plastic shake down from the

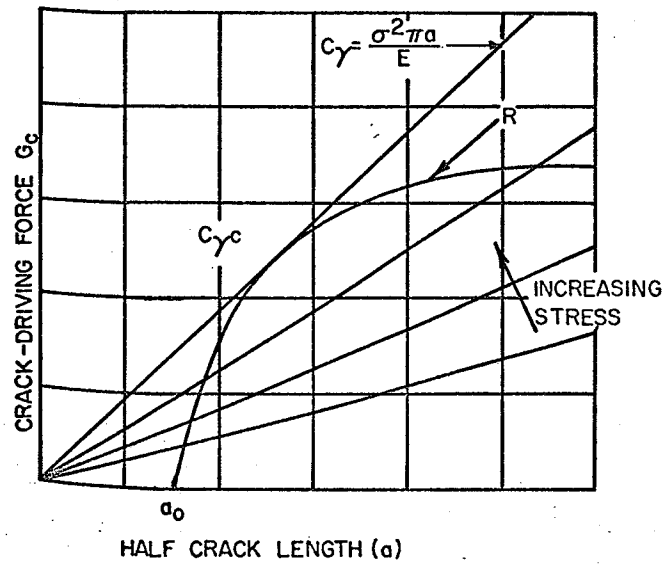


FIGURE 2.15 THE CONCEPT OF FRACTURE GROWTH UNDER A STATIC LOAD

initial state will occur after a few cycles. Therefore, the resistance to crack growth will be mainly dependent on the alternating stress. It is assumed that most, if not all, of the crack growth will occur at the maximum stress of the cycle and hence the crack driving force will be dependent on the maximum stress.

A sketch of the proposed mechanics of fatigue crack growth under constant load cycle proposed by Cotterell (13), is shown in Figure 2.16. As the crack grows to length l_1 ;

$$R(l_1 - l_0) = G(l_1) \quad \dots 2.2$$

During the next cycle the crack grows by slightly larger amount to

$$R(l_2 - l_1) = G(l_2) \quad \dots 2.3$$

This growth continues until the penultimate cycle when the crack is of length l_{n-1} . Then in the ultimate cycle, it grows to l_n and fracture occurs. In practice the crack growth per cycle is very small compared with the crack length and the equation for growth can be written in the limiting form:

$$R\left(\frac{\Delta l}{\Delta N}\right) = R\left(\frac{dl}{dN}\right) = G(l) \quad \dots 2.4$$

For small rates of crack growth the rate is proportional to the crack length.

$$\frac{dl}{dN} = \frac{\sigma_a^2 \pi l}{E R'(0)} \quad \dots 2.5$$

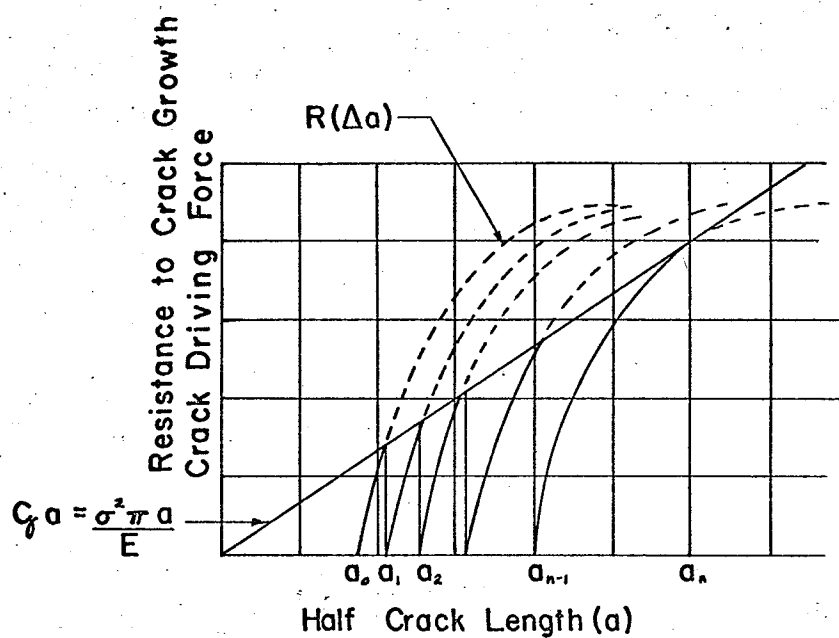


Figure 2-16 The Concept of Fracture Growth Under Repeated Loads

where $R'(0)$ is the first derivative at $dl/dN = 0$

The expression used for the crack driving force, equation 2.1, is for a central crack in an infinite elastic plate under uniform stress and needs modification for the effects of plasticity and finite width of the plate. Allowance for these effects have been suggested by Irwin (14) for the case of static loading and it is thought that these can be applied directly to fatigue.

From inspection of the elastic field equations, Irwin (14) has estimated that the size of the plastic zone is

$$d = \frac{GE}{\pi \sigma_y^2} \quad \dots 2.6$$

where σ_y is the yield stress of the material.

Frost and Dugdale (15) show that for fatigue, the plastic zone is also dependent on the maximum stress. The existence of the plastic zone modifies the elastic field beyond the zone roughly as though the crack length were increased by a fraction of the plastic zone. Irwin (14) suggested, from experimental observations and considerations of equilibrium, that the effective crack length should be the actual crack length plus the plastic zone.

$$l' = l + d \quad \dots 2.7$$

Hence substituting equation 2.1 and 2.6 in equation 2.7,

$$l' = l + \frac{1}{2} \left(\frac{\sigma_0}{\sigma_y} \right)^2 l' \quad \dots 2.8$$

and

$$l' = \frac{l}{1 - \frac{1}{2} \left(\frac{\sigma_0}{\sigma_y} \right)^2} \quad \dots 2.9$$

Therefore, providing that the crack is small compared with the width of the plate, the plastic zone is

$$d = \frac{(\sigma_0/\sigma_y)^2}{1 - 0.5(\sigma_0/\sigma_y)^2} a \quad \dots 2.10$$

The expression is compared in Figure 2.17 with the experimental results of Frost and Dugdale (15) and their suggested relationship $d/l = C \sigma_0^3$.

Where C is a material constant. The equation 2.5 is modified for the effect of the plastic zone and the expression for the rate of crack propagation becomes

$$\frac{dl}{dN} = \frac{\sigma_0^2 l}{1 - 0.5(\sigma_0/\sigma_y)^2} \left\{ \frac{\pi}{E \bar{R}'(0)} \right\} \quad \dots 2.11$$

An experimental and analytical investigation was undertaken by Liu (16) to study the fundamental factors of crack propagation in a thin metal sheet under repeated axial loading. Sheet specimens of 2024-T3 aluminum alloy containing centre holes were used. Crack propagation in the semi-infinite plate under constant stress range and mean stress was analyzed using dimensional analysis.

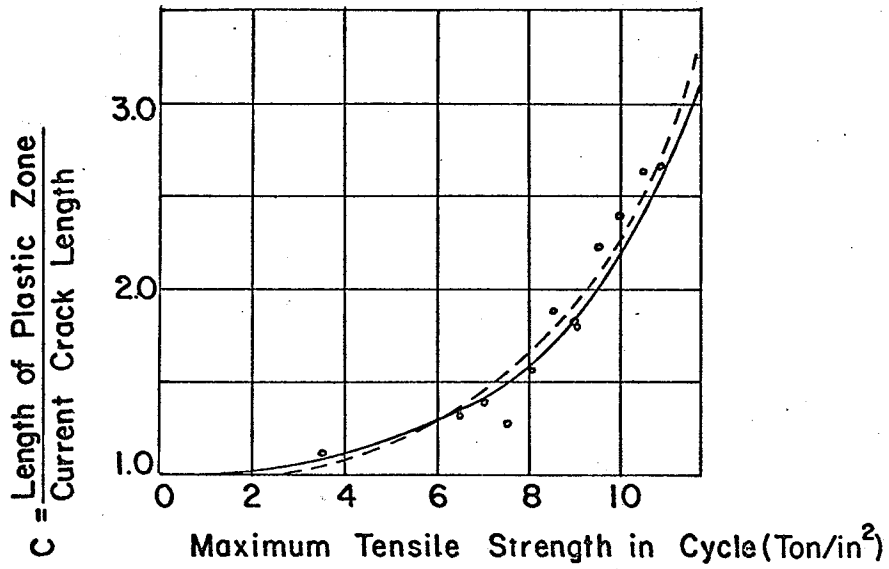
A thin material of thickness t and width L , containing a crack of length l , as shown in Figure 2.18, was loaded axially by a combination of a constant amplitude repeated stress σ_0 is shown acting on the specimen in Figure 2.18.

Neglecting the microscopic variables, the stress $\sigma_\theta(x, y)$ at point $P(x, y)$ in the direction of θ can be written as

$$\sigma_\theta(X, Y) = F(\sigma_0, X, Y, \theta, t, L, B_1, B_2) \quad \dots 2.12$$

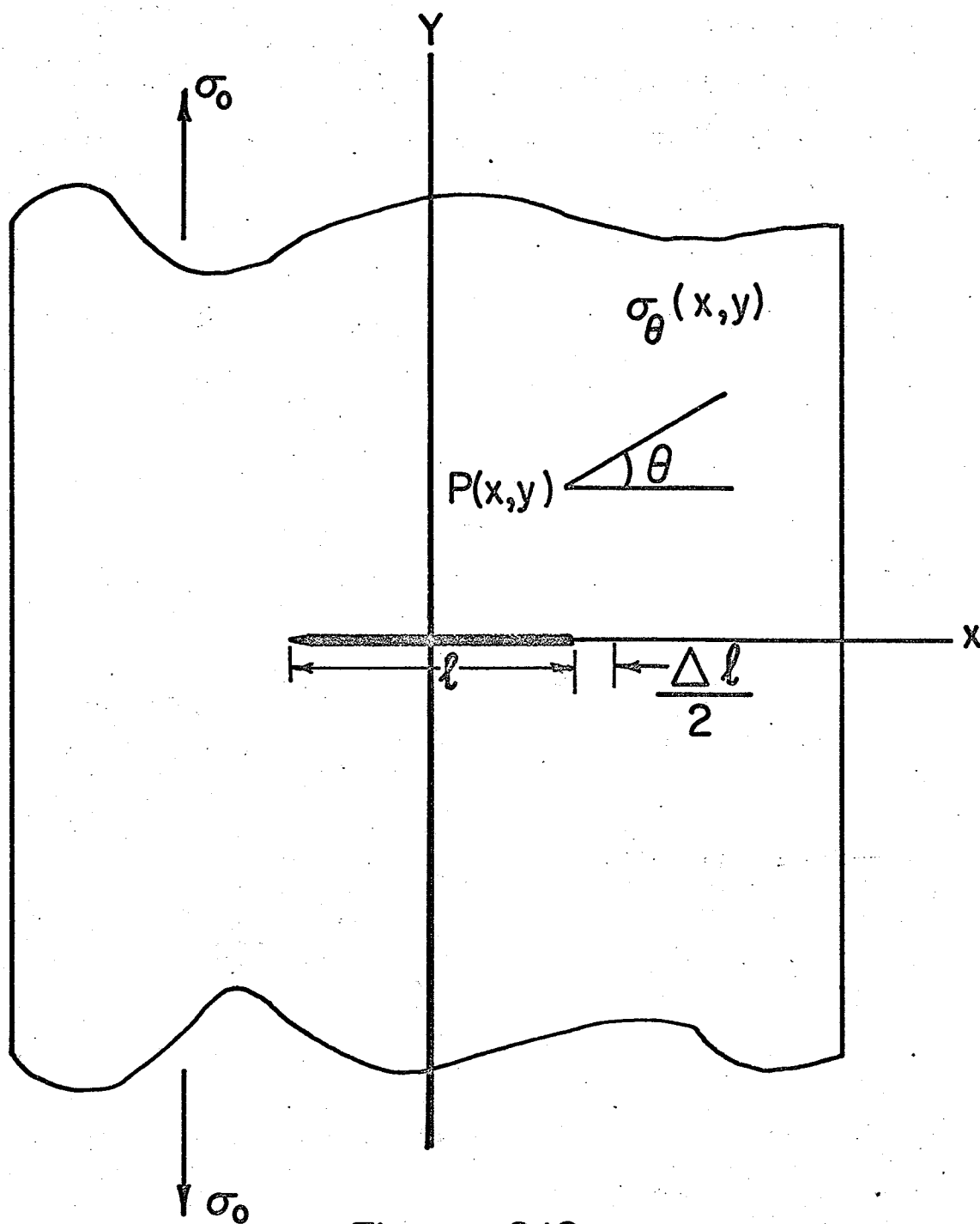
B_1 = Configuration of crack

B_2 = Complete stress-strain relationship



- Experimental Points Frost & Dugdale (8)
- $C = 1 + 0.0013 \sigma_0^3$
- $C = 1 + \frac{(\frac{\sigma_0}{\sigma_y})^2}{1 - \frac{1}{2} (\frac{\sigma_0}{\sigma_y})^2}$

Figure 2-17 Ratio of Length of Plastic Zone to Crack Length for Mild Steel



Schematic diagram of a section of an axially loaded sheet specimen.

If plane stress is assumed and the width, L , is large relative to the crack length, l , the variables t and L can be excluded. If the shape of the crack for a given value of σ_0 remains geometrically similar, and is independent of the crack length, the configuration of the crack can be specified by crack length alone. Therefore, equation 2.12 can be written as

$$\sigma_0(X, Y) = F(\sigma_0, X, Y, \theta, l, B_2) \quad \dots 2.13$$

To study the similarity of the two specimens, consider a "model" and a "prototype" of the sheet of material containing a crack. Let nominal stress σ_0 be same for both model and prototype. If Δl_1 and Δl_2 and homologous increments of crack length, where subscripts 1 and 2 denote model and prototype, respectively. Then by dimensional analysis they must satisfy the condition

$$\frac{\Delta l_1}{l_1} = \frac{\Delta l_2}{l_2} = C_1 \quad \dots 2.14$$

then the number of cycles of load, ΔN , to propagate a crack length

Δl_1 and Δl_2 must be the same if the mechanics of crack growth is the same for both cases. Therefore, equation 2.14 can be written as

$$\frac{\Delta l_1}{l_1 \Delta N} = \frac{\Delta l_2}{l_2 \Delta N} = C \quad \dots 2.15$$

Where C is the crack propagation factor.

Now considering subscripts 1 and 2 as two stages in the course of crack propagation through one specimen rather than crack propagation in two similar specimens, equation 2.15 describes the basic law of crack propagation in a thin semi-infinite sheet. Writing equation 2.15 in

differential and integral form give,

$$\frac{dl}{dN} = C l \quad \dots 2.16a$$

and

$$\text{Log } l - \text{Log } l_0 = C(N - N_0) \quad \dots 2.16b$$

Liu (17) further showed by energy approach that

$$\text{Log } \frac{1}{I_0} = K S^2 (N - N_0) \quad \dots 2.17$$

where ΔS is stress range. Equation 2.17 indicates that the fatigue crack propagation rate is proportional to ΔS^2 .

Comparing equation 2.16a and 2.17 indicates that the crack propagation factor C is related to the stress range ΔS by

$$C = K \Delta S^2 \quad \dots 2.18$$

Figure 2.19 is the logarithmic plot of crack propagation factor C of 2024-T3 aluminum alloy against the stress range ΔS .

Head (3, 4) proposed that the crack grows through material whose ductility has been exhausted by strain hardening. He assumed that the effect of reversed plastic strains are additive as are unidirectional strains. However, the rate of hardening is very sensitive to the amplitude of the reversed strains. To calculate the behaviour at the tip of the crack, Head used a model composed of sets of three elements representing: (1) plastic flow, (2) elastic restraint, and (3) interaction between the sets of elements. From this model he derived the expression

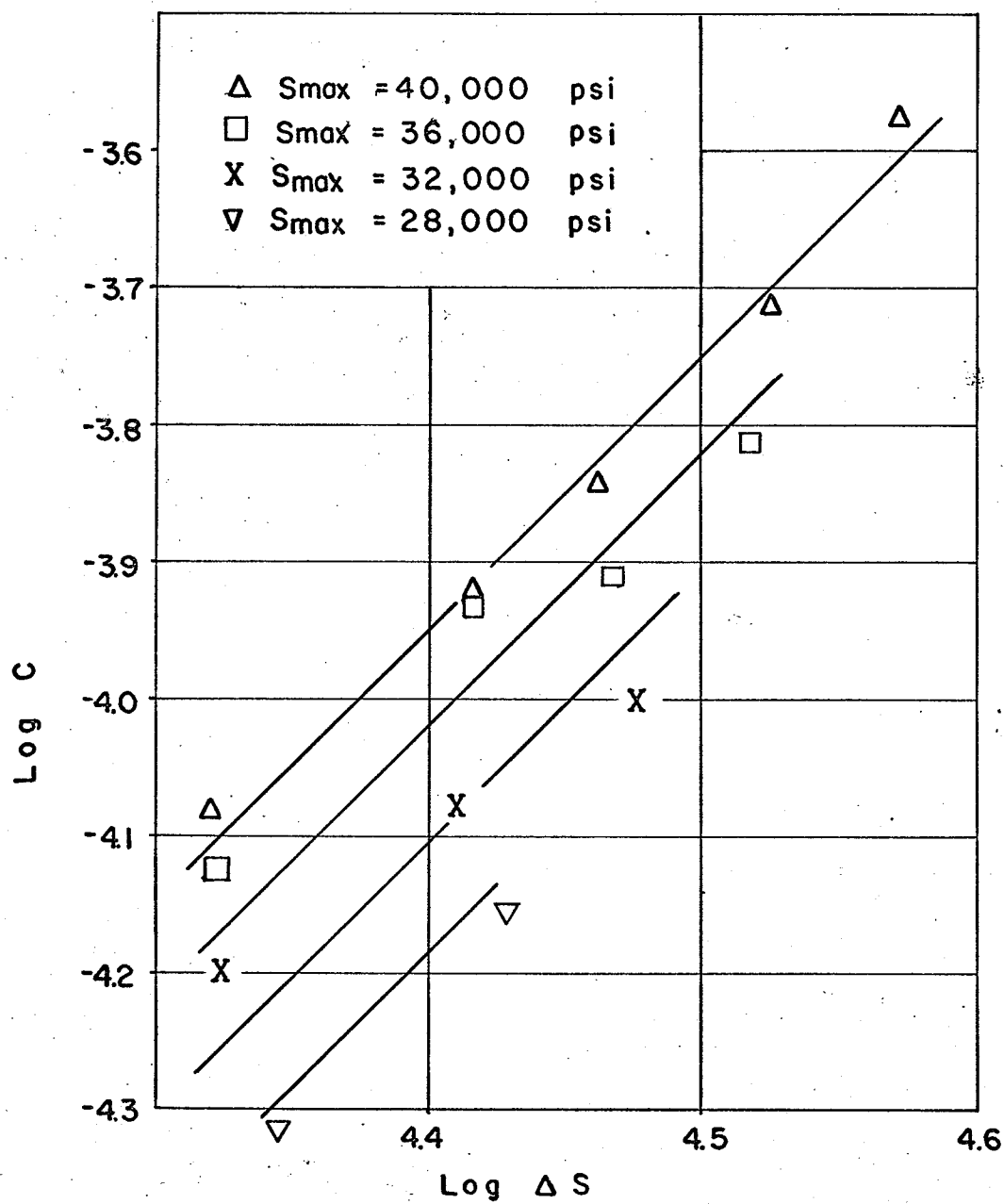


Figure 2-19 Correlation Between Crack Propagation Factor and Stress Range

$$\frac{da}{dN} = a^{3/2} d^{-1} f(\sigma_A) \quad \dots 2.19$$

where, a , is the half-crack length, N , the number of cycles, d , the thickness of the plastic zone, and $F(\sigma_A)$ a function of the alternating stress. Head assumed that the plastic zone was independent of crack length and thus decided that a varied inversely with N , but as Frost and Dugdale (19) have shown, the thickness of the plastic zone is proportional to the crack length. Thus

$$\frac{da}{dN} = Ka \quad \dots 2.20$$

where K is stress dependent. Frost and Dugdale have obtained an empirical expression for K

$$K = A \sigma_A^3 \quad \dots 2.21$$

where A is a material constant dependent, in some materials on the mean stress.

McEvily and Illg (20) approached the crack propagation problem in a similar way to Head (3, 4). They assumed that a crack lies dormant for ΔN cycles while the region at the tip of the crack strain hardens sufficiently for the crack to grow through a small distance Δa . Their theory is then developed in functional form assuming that both the rate of strain hardening and the distance Δa through which the crack grows are dependent on the maximum stress at the tip of the crack. McEvily and Illg use an effective stress concentration factor K_N which is almost proportional to the square root of the crack length, to calculate the stress at the tip of the crack. From experimental results on

two aluminum alloys tested at a load range $\beta = 0$, they found the functional relationship

$$\text{Log } \frac{\Delta a}{\Delta N} = 0.0059 K_N \sigma_0 - 5.472 - \frac{34}{K_N \sigma_0 - 34} \quad \dots 2.22$$

where σ_0 is the maximum applied stress calculated on the basis of the remaining cross-sectional area. In a later paper (21) they showed that the same relationship, except for a minor adjustment, held when the alloys were tested under completely reversed loading ($\beta = -1$) and thus concluded that the main factor influencing fatigue crack growth was the tension part of the cycle.

McEvily and Illg (20) compared their theory with that of Head (3) and found agreement for short cracks. A comparison has been made with the theory of Frost and Dugdale (19). For moderate crack lengths there is agreement, but for very small cracks equation 2.22 reduces to

$$\text{Log } \frac{\Delta a}{\Delta N} \propto \sigma_0 a^{1/2} \quad \dots 2.23$$

and McEvily and Illg's theory predicts a smaller rate of growth.

In service, the majority of structures are subjected to some degree of multiaxial or biaxial stress. However, the major emphasis in the evaluation of fatigue resistance in the laboratory is on the uniaxial loading methods.

Metal fatigue under multiaxial strain is a complex phenomena. Losses in ductility and anisotropy, as well as texture hardening of materials, contribute to the complexity of the problem, but the effect of these factors on biaxial fatigue properties have not been properly investigated. Empirical characteristics defined for one material do not

necessarily apply for other materials since: (1) some materials have greater tensile strengths in the longitudinal rolling direction, while in others, it is in the transverse direction: (2) many unflawed materials with higher biaxial strengths than uniaxial strengths show a higher uniaxial than biaxial strength when flawed; and (3) for certain stress ratios, the maximum principal strain may be normal to the weakest axis of the material but, when the stress ratio is altered, becomes normal to the strongest axis of the material.

2.8. Summary

An outstanding feature of the existing literature is it's divergency of approaches to the propagation of fatigue cracks. The ultimate goal is a synthesis of the various approaches in order to arrive at a mere complete understanding of the crack growth phenomenon.

The divergency of the papers is illustrated by the different starting points adopted by the authors:

- 1) Engineering approach versus the theoretical approach.
- 2) Empirical data versus microstructural studies
- 3) Technical materials versus pure metal.
- 4) Macroscopic observations versus microscopic observations.

CHAPTER 3

Development of Biaxial Fatigue Crack Propagation Theory

3.1 Introduction

The majority of structures are subjected to some degree of multiaxial or biaxial stress. However, the major emphasis in the evaluation of structures for fatigue resistance in the laboratory is on uniaxial loading methods. In many applications, the indiscriminate use of uniaxial data will result in unconservative design and premature structural failure.

Metal fatigue under multiaxial stress or strain is a complex phenomenon. Losses in ductility and anisotropy as well as texture hardening of materials, contribute to the complexity of the problem, but the effects of these factors on biaxial fatigue properties have not been fully investigated. Empirical characteristics defined for one material do not necessarily apply for other materials. In a few cases in the past, although the material property peculiarities were known they were neglected in design with catastrophic results to the structure.

In this chapter a theory is proposed for the effects of the degree of biaxiality of stress on the rate of fatigue crack propagation.

3.2 Uniaxial Fatigue Crack Propagation Theory

A form of semiempirical expression was developed by McEvily and Illg (21) for a stress range of σ_o up to 50 ksi and minimum nominal stress of 1 ksi. Illg and McEvily (20) extended this work to completely reversed loading. Sheet specimens of 2024-T3 and 7075-T6 aluminum alloys were tested.

The process of fatigue crack propagation was considered to comprise two stages as in reference (3). During the first stage, the material in a critical region at the tip of a crack is cyclically work-hardened up to the fracture strength of the material; during the second stage the crack is propagated an incremental amount into material which has not been fully work-hardened. Then the first stage is repeated, and so forth.

The first stage process of work-hardening at the tip of the fatigue crack is considered to involve both the Orowan (22) concept and the findings of Wood and Segall (23), with the addition that the stress concentration factor for the crack K_N is taken into account.

In order to formulate an expression for the rate of fatigue crack propagation, let n be the number of cycles elapsed in a particular stage 1 upon which attention has been focused since the preceding stage 2, and let ds/dn be interpreted as the rate of increase of stress per cycle at a critical site during this first stage. Denote the total number of cycles involved from the start to the finish of this stage by ΔN . Then the total number of cycles to propagate a crack over some large distance will be the sum of the various values of ΔN involved, if no cycles are involved in the second stage. If it is assumed that the rate of stress at the critical site is inversely proportional to the number of cycles n since the last increment of crack growth and that the rate for a propagating crack also depends upon $K_N S_{NET}$ and the endurance limit, the rate of increase of stress can be expressed as

$$\frac{d\sigma}{dN} = \frac{1}{N} F(K_N S_{NET}, S_e) \quad \dots 3.1$$

When this expression is integrated between the local yield strength σ_y , and the local fracture strength σ_f , the following expressions are obtained:

$$\text{Log } \Delta N = F_1(K_N S_{NET}, S_e) \int_{\sigma_y}^{\sigma_f} d\sigma \quad \dots 3.2$$

or

$$\text{Log } \Delta N = F_1(K_N S_{NET}, S_e) \times C_1 \quad \dots 3.3$$

Therefore

$$\Delta N = e^{C_1 F_1(K_N S_{NET}, S_e)} \quad \dots 3.4$$

The extent of incremental crack growth during the second stage also depends upon the value of $K_N S_{NET}$ and may be expressed as;

$$\Delta X = F_2(K_N S_{NET}) \quad \dots 3.5$$

It is assumed that the time required for this incremental growth is small compared with the period of cycling. The average rate of fatigue crack propagation may be expressed as

$$r = \frac{\Delta X}{\Delta N} = \frac{F_2(K_N S_{NET})}{e^{C_1 F_1(K_N S_{NET}, S_e)}} \quad \dots 3.6$$

or

$$\text{Log}_{10} r = \text{Log}_{10} F_2(K_N S_{NET}) - \frac{C_1}{2.3} F_1(K_N S_{NET}, S_e) \quad \dots 3.7$$

3.3 Octahedral Shear Stress Theory

The octahedral shear stress theory or distortion energy theory was originated by Huber in 1940 (24). It can be expressed mathematically in many ways. One form is

$$(\tau_{\text{oct}})_y = (\tau_{\text{oct}})_o \quad \dots 3.8$$

where τ_{oct} is the shear stress acting on the octahedral plane, i.e., that making equal angles with the principal stress axis. The left side represents the stress for yielding in any state, while the right side is that for simple tension.

The octahedral shear stress given by Timoshenko (25) is

$$\tau_{\text{oct}} = \frac{1}{3} \sqrt{(\sigma_1 - \sigma_2)^2 + (\sigma_2 - \sigma_3)^2 + (\sigma_3 - \sigma_1)^2} \quad \dots 3.9$$

To evaluate this expression for yielding in simple tension, let $\sigma_1 = \sigma_y$ and $\sigma_2 = \sigma_3 = 0$, from which

$$(\tau_{\text{oct}})_o = \frac{\sqrt{2}}{3} \sigma_y \quad \dots 3.10$$

substituting in equation 3.8 we obtain, in accordance with the octahedral shear stress theory,

$$(\sigma_1 - \sigma_2)^2 + (\sigma_2 - \sigma_3)^2 + (\sigma_3 - \sigma_1)^2 = 2 \sigma_y^2 \quad \dots 3.11$$

3.4 Biaxial Fatigue Crack Propagation Theory

This theory is a modification of the uniaxial fatigue crack propagation theory developed by McEvily and Illg (21) and octahedral shear stress theory.

Irwin's (26) stress intensity factor K reflects the effect of external load and configuration on the intensity of the whole stress field around a crack tip. Moreover, for various configurations the crack tip stress field always has the same form. Therefore, it was reasoned that the intensity of the crack tip stress fields as represented by K should control the rate of crack growth. That is to say:

$$\frac{da}{dN} = G(K) \quad \dots 3.12$$

For biaxial stress fields this representation is rather useful, since the effect of biaxiality of stress can now be incorporated in the evaluation of the stress intensity factor K in such way that it could be used for uniaxial as well as biaxial conditions.

The choice of octahedral shear stress theory is based on the fact that many authors, Shewchuk (27), Majors, Mills and MacGregor (28), have found it suitable for biaxial fatigue theories.

For a crack traversing a plate it was observed by Paris (29),

$$K = \sigma_a^{1/2} \quad \dots 3.13$$

Substituting equation 3.13 in 3.12 obtain:

$$\frac{da}{dN} = G(\sigma_a^{1/2}) \quad \dots 3.14$$

Hardrath (30) observed that K_{NET} for the configuration considered here is

$$K_{NET} = \sigma \left[1 + 2(a/\rho)^{1/2} \right] \quad \dots 3.15$$

where ρ is the radius of the crack tip.

similar to the stress intensity factor, equation 3.13

$$K = \sigma a^{1/2} \quad \dots 3.16$$

if ρ_i is small compared to crack length, a . For aluminum alloys, namely 2024-T3 and 7075-T6 McEvily and Illg (20) observed that ρ_i is less than 0.005 inch. So that the condition $\rho_i \ll a$ is present for crack of readily observable length in crack propagation tests.

For biaxial stress conditions, the stress intensity factor K is proportional to τ_{oct}

$$K = \tau_{oct} a^{1/2} \quad \dots 3.17$$

McEvily and Illg (20, 21) conducted uniaxial fatigue crack propagation tests on 2024-T3 aluminum alloy and derived a form of semi-empirical equation 3.7

$$\text{Log}_{10} \gamma = \text{Log}_{10} F_2(K_N S_{NET}) - \frac{C_1}{2.3} F_1(K_N S_{NET}, S_e) \quad \dots 3.18$$

An equation which fits the test data and incorporates equation 3.18 is

$$\text{Log}_{10} \gamma = A_1 K_N S_{NET} + A_2 + A_3 \frac{S_f}{K_N S_{NET} - S_f} \quad \dots 3.19$$

Substituting the stress intensity factor K from equation 3.17 for $K_N S_{NET}$ in equation 3.19, a general form of biaxial fatigue crack propagation equation is obtained:

$$\text{Log}_{10} \gamma = A_1 + A_2 + A_3 \frac{\tau_{oct}}{A_4 K - \tau_{oct}} \quad \dots 3.20$$

where $\tau_{oct} = \frac{\sqrt{2}}{3} S_f$, and S_f is the fatigue limit of the particular material.

CHAPTER 4

Experimental Study

4.1 Introduction

Most of the investigations in fatigue crack propagation have utilized uniaxial stress or strain cycling. There is little data available for biaxial stress conditions. A theory for predicting biaxial fatigue crack propagation has been presented in Chapter 3. To check the validity of the proposed theory a testing program for biaxial stress cycling with various biaxiality of stress was carried out. All the tests were conducted with the major principal stress constant.

4.2 Material and Specimens

The material used was 2024-T351 aluminum alloy rolled plate with a nominal thickness of 0.250 inch. The chemical composition and mechanical properties as supplied by the manufacturer are given in Table 4.1 and 4.2 respectively. The specimens were surface polished by 400 grit and 600 grit Silicon Carbide paper.

As shown in Figure 4.1, three series of specimens were made, each having different surface principal stress ratio. The direction of rolling was along the major axis for all specimens. The strain and stress ratios are given in Table 4.3. All specimens were cut out by a band saw. A total of 24 specimens was made for calibration and testing.

Table 4-1

Chemical Composition of 2024-T351 Aluminum Alloy

Zn - 0.1%

Mg - 1.5%

Cu - 4.2%

Cr - 0.1%

Mn - 0.6%

Table 4-2

Mechanical Properties of 2024-T351 Aluminum Alloy

Ultimate tensile strength - 71,000 psi

Tensile yield strength - 48,000 psi

Elongation at rupture - 18% for 2 inch gauge length.

Young's modulus - 10×10^6 psi

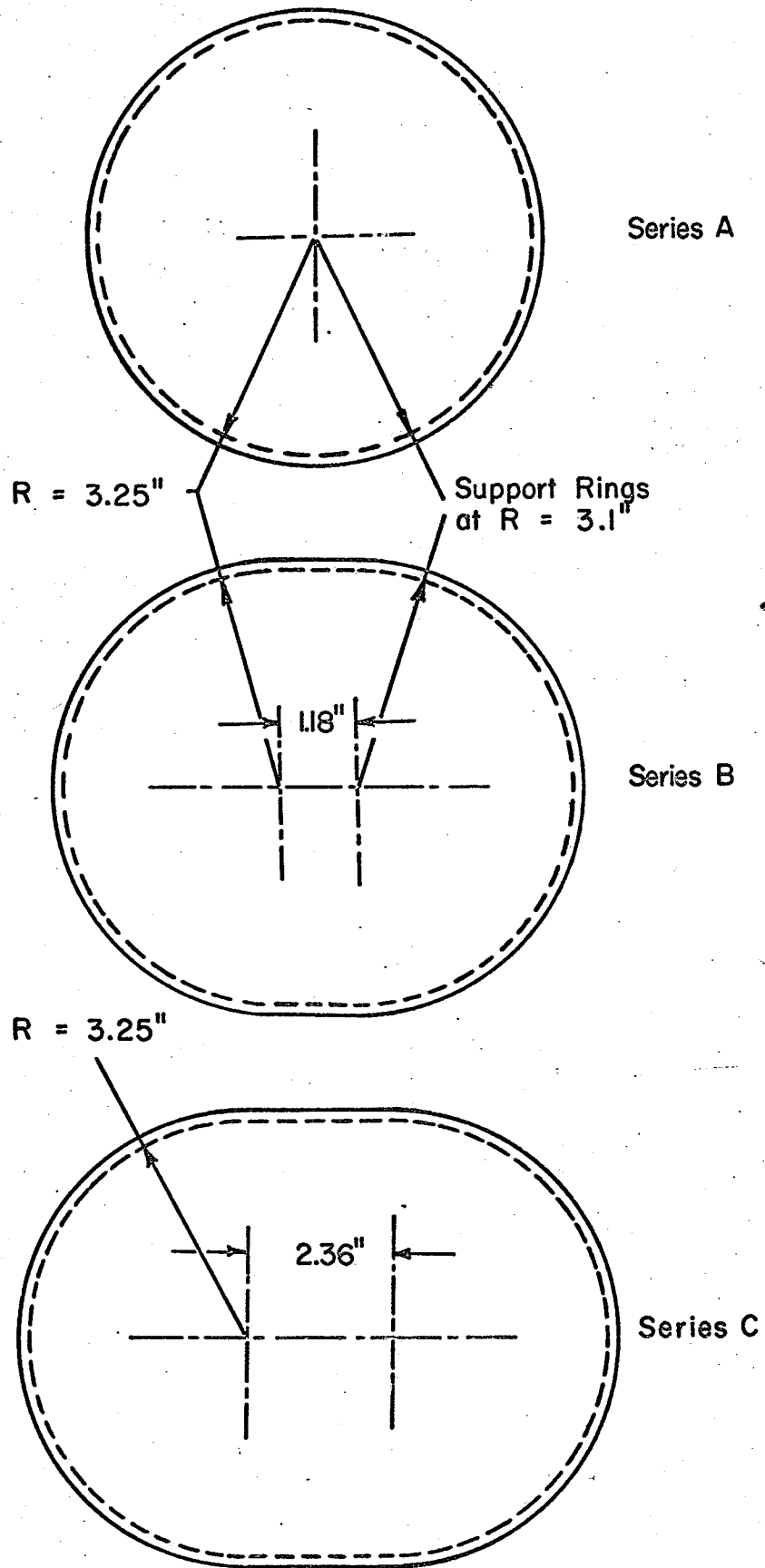


Figure 4.1 Specimen Dimensions

Table 4-3

Description of Specimens

<u>Series</u>	<u>*Stress Ratio</u>	<u>Type of Specimen</u>
A	1:1	Round plate
B	1:0.86	Double semicircular plate
C	1:0.75	Double semicircular plate

* Ratio of maximum to minimum surface principal stresses,

Maximum principal stress σ_1 for all specimens

is constant, $\sigma_1 = 41,000$ psi

4.3 Test Equipment

A machine designed on a similar principle as that of Shewchuk (27), was built and is shown in Figure 4.2. Figure 4.3 is a schematic diagram of the machine.

The specimens in the plate bending machine were hydraulically pressurized on alternate sides through a reversing four-way solenoid controlled valve.

The direction of flow in the solenoid valve was governed by pressure switches one for each side of the plate. The electrical control circuit diagram is shown in Figure 4.4. As the pressure is increased on one side of the plate, the pressure switch would denenergize one relay at a set pressure and at the same time energize the second relay, thereby changing the flow of current from one solenoid to the other one and thus reversing the fluid flow. A similar function was performed by the second pressure switch. The stress in the plate specimens could be changed by adjusting the pressure switch setting for different pressure. A detailed description of the equipment is given below.

1. Plate Testing Machine

Three main components make up the plate testing machine. These are the pressure chamber, the specimen holder and the pressure control circuit.

1.1 Pressure Chamber

The pressure chamber is a semi-enclosure of two spaced, parallel steel plates with two open ends. This construction is unique in that the specimen holder could be slid into the chamber through the open end as shown in Figure 4.5. The specimen can then be secured in place

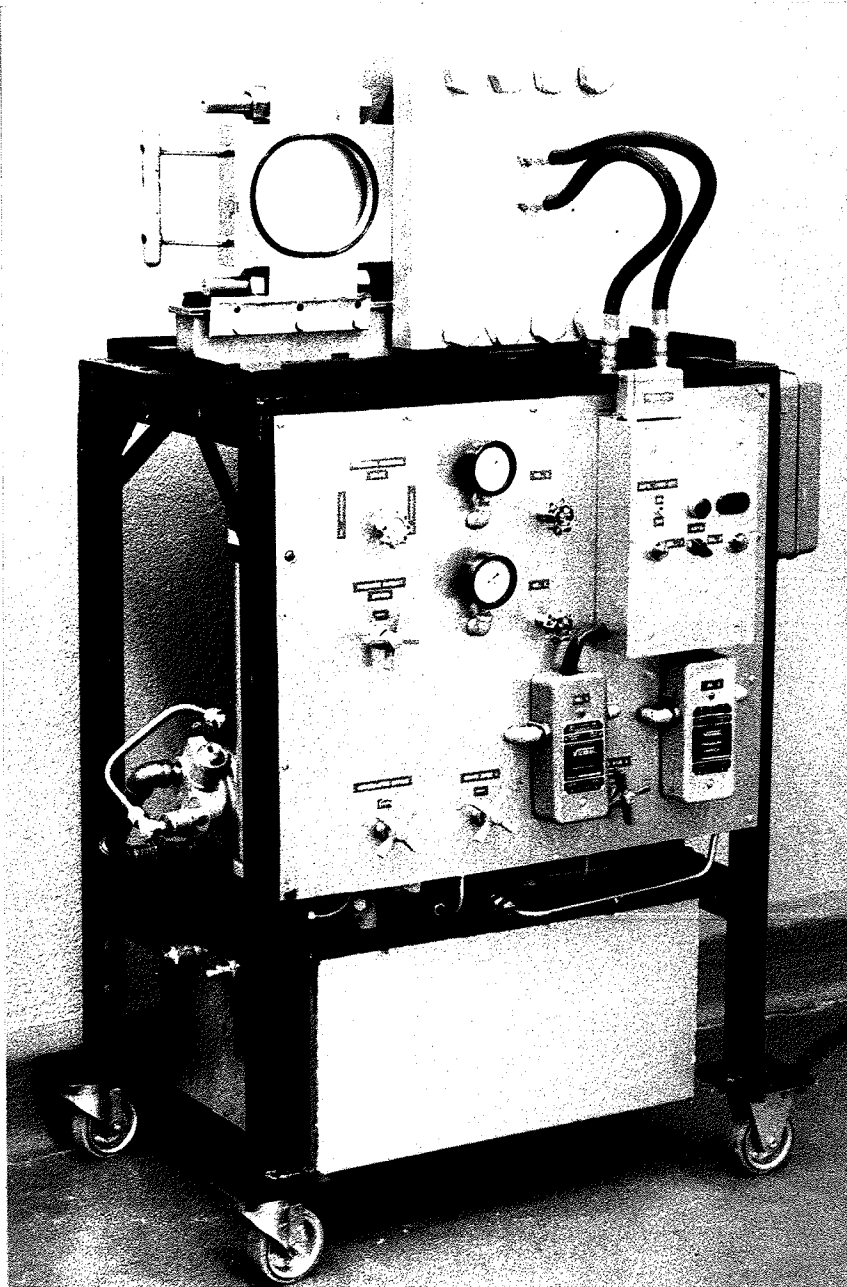


Figure 4.2 Test Equipment

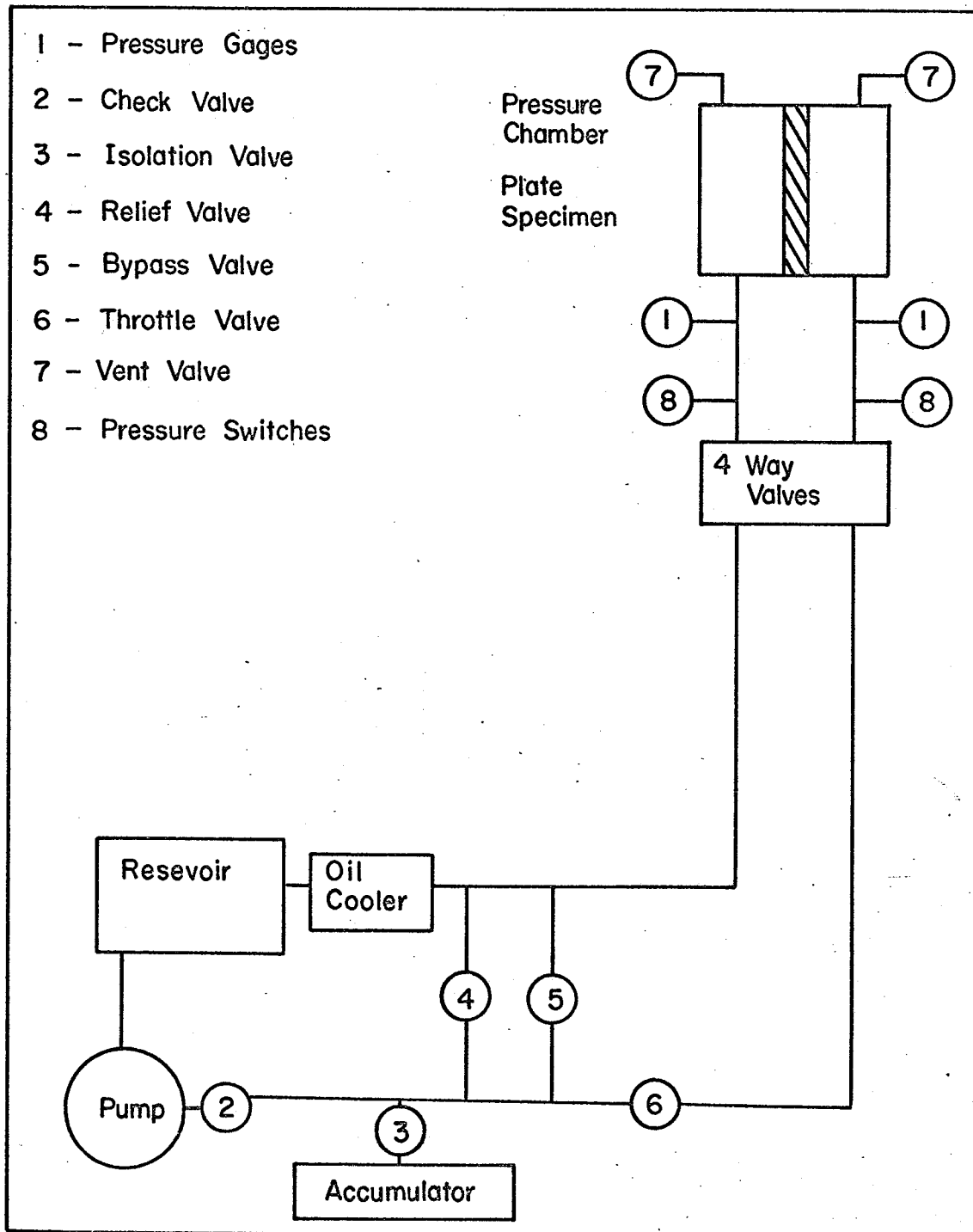


FIGURE 4.3 SCHEMATIC DIAGRAM OF TESTING MACHINE

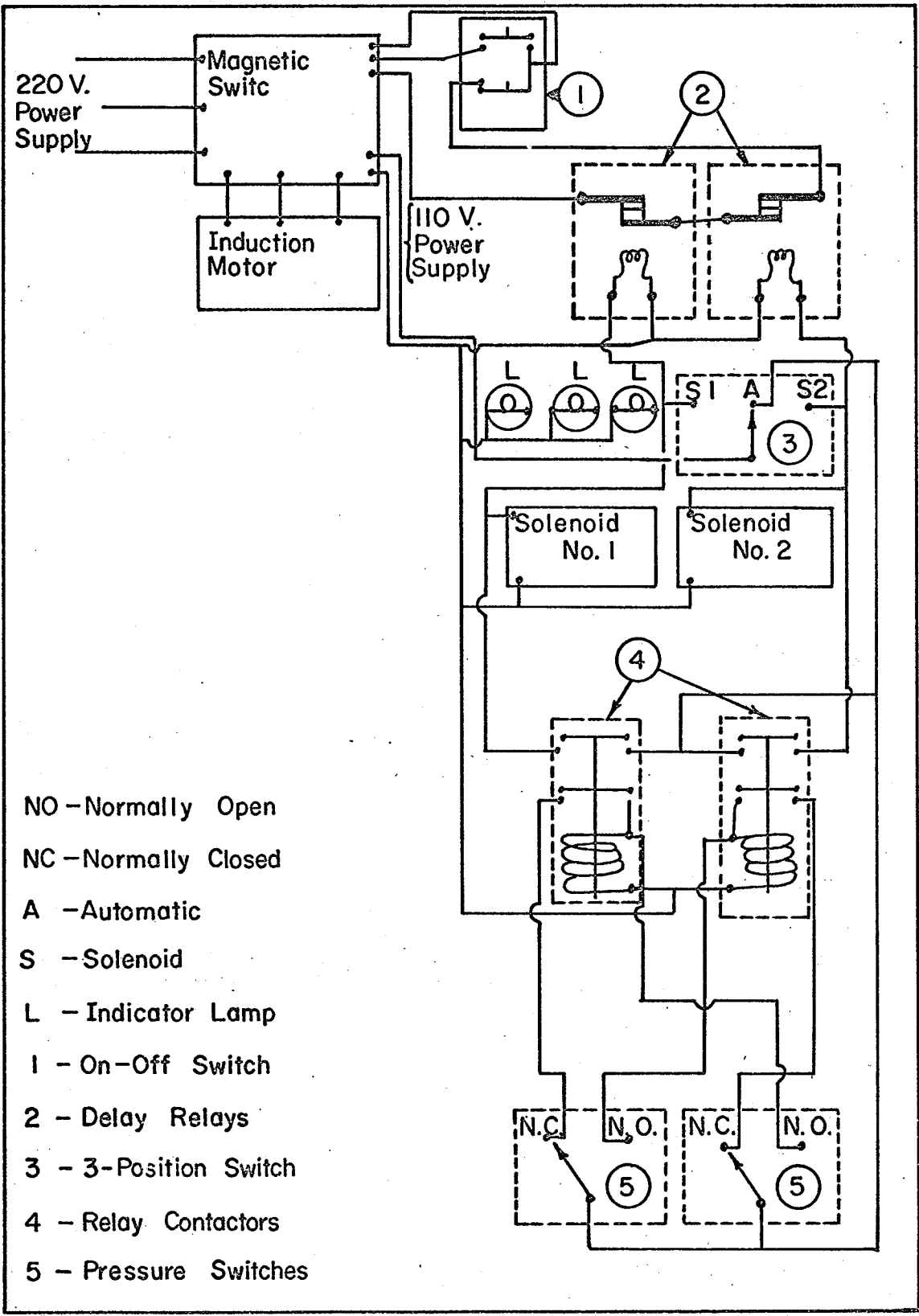


Figure 4.4 Electrical System for Biaxial Fatigue Machine

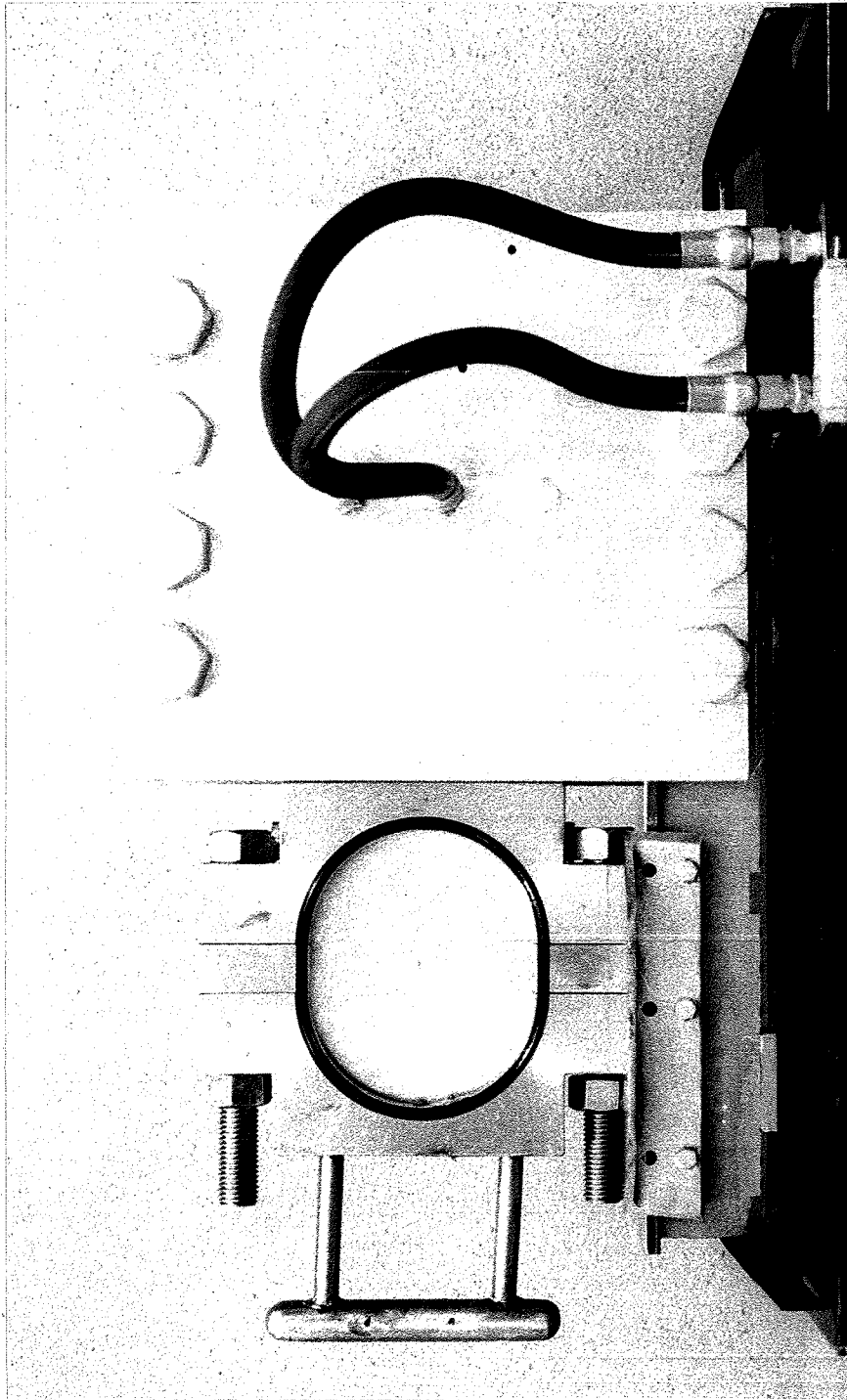


Figure 4.5 Opening End of Pressure Chamber

by simply tightening the eight retaining bolts. Pressure and vent ports are located in each of the two plates at the centre and high point of the positioned specimen holder opening to permit efficient venting of the chamber.

1.2 Specimen Holder

Another unique feature of the plate bending machine is the construction of the specimen holder. As shown in Figure 4.6, the holder is a pair of inside semicircular blocks with a cross-sectional retaining groove for the specimen, specimen support rings and pressure seals. By bolting the two blocks together, a round plate specimen can be enclosed. However, by using matched pairs of grooved spacing blocks, the holder can be modified to simply support the double semicircular plates. In accordance with the specimen dimensions as shown in Figure 4.1, two sets of spacing blocks, 1.18 and 2.36 inches long were made.

Sealing of the specimens was accomplished as shown in Figure 4.7 Quad-rings were used in sealing the specimen holder in the pressure chamber and the specimen was sealed in the transverse groove also by quad-rings. Some leakage was observed around the specimen but no effort was made to eliminate it, as this had no adverse effect on the experiment.

The specimens were simply supported on butt welded rings of 3/16" diameter steel rod ground on one side to reduce the thickness of the rings to 0.170 ± 0.03 ". This way sufficient clearance was allowed between rings to allow for rotation of the specimen at the support.

1.3 Pressure Monitor

Figure 4.4 illustrates the operation of the pressure control circuit. One pressure switch is connected to each side of the pressure

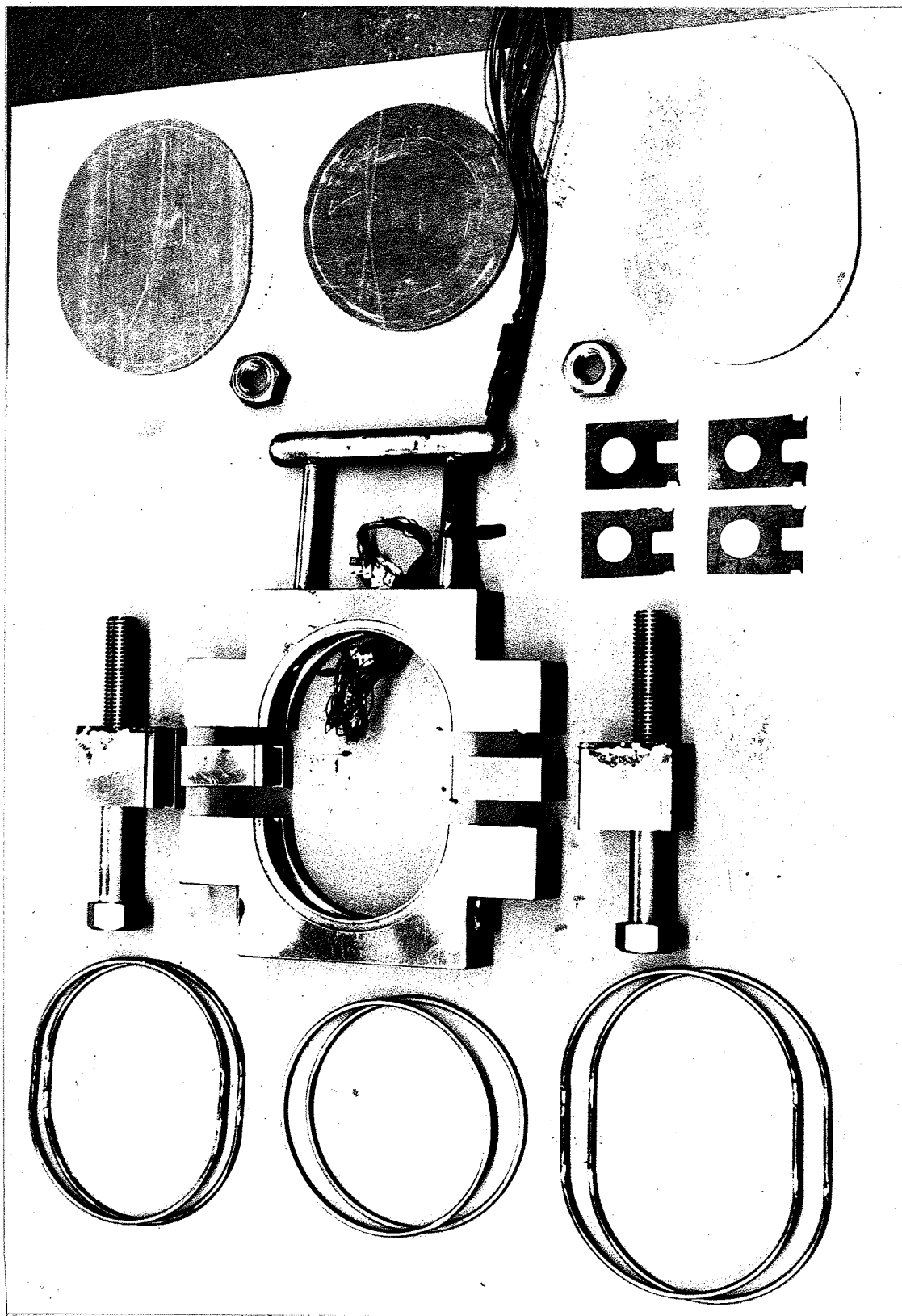


Figure 4.6 Exploded View of Specimen Holder

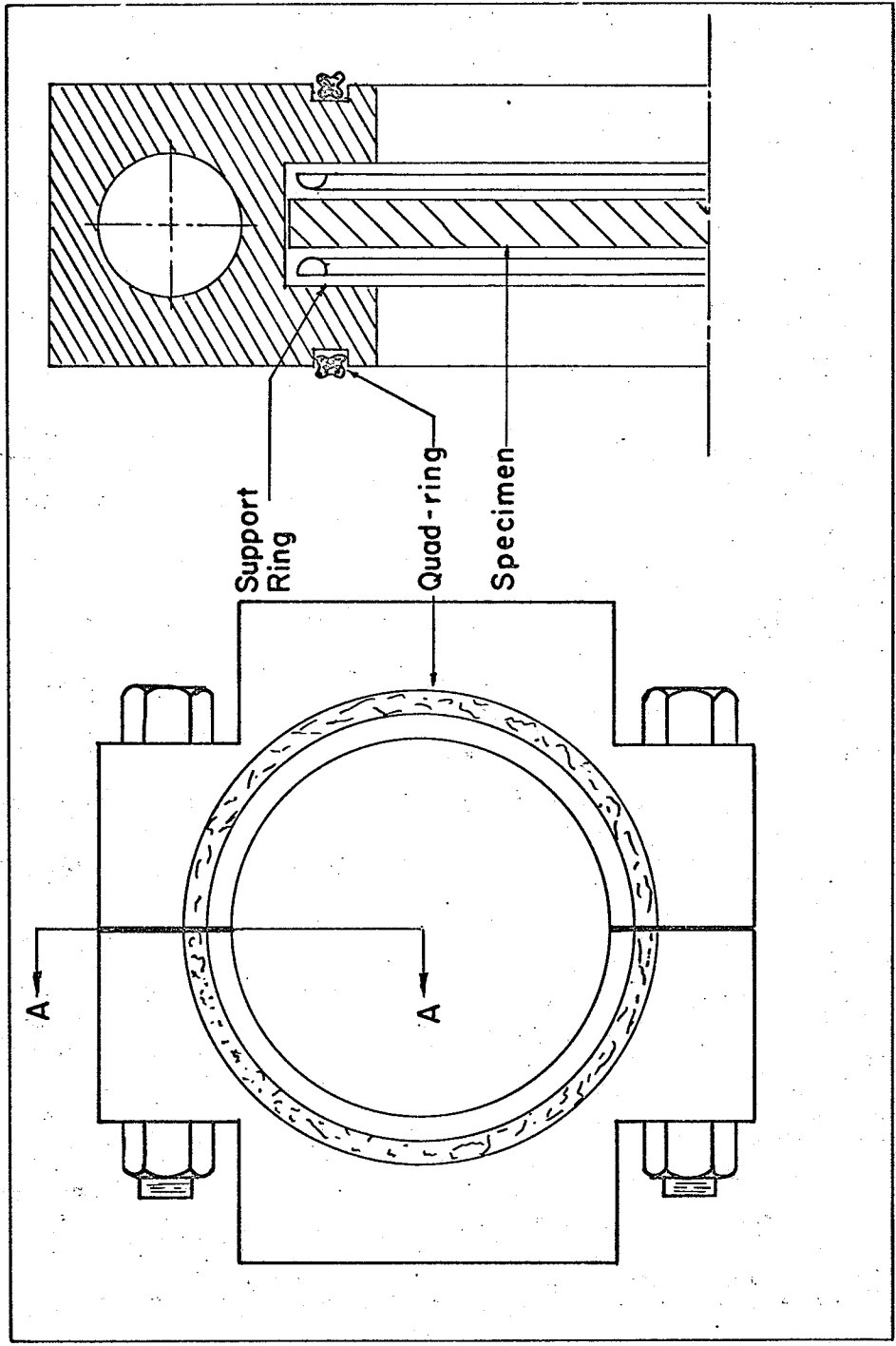


Figure 4.7 Specimen Holder and Seals

chamber. The pressure switch has a two position microswitch which is normally closed by the pressure of a spring. This spring pressure can be varied from 50 psi to 2,000 psi. The oil pressure in the respective pressure chambers acts against the spring pressure. When the oil pressure exceeds the spring pressure the microswitch is thrown open. The microswitch is accurate within ± 5 psi. of the set pressure.

The action of a microswitch is used to energize and de-energize the relays which control the electric current to the solenoid coils. When pressure in the pressure chamber 1 reaches the set pressure the microswitch 1 is thrown open, thereby de-energizing relay 1 and at the same energizing relay 2. Now the electric supply is changed from solenoid 1 to solenoid 2 of the 4-way valve. This leads to changing the flow of high pressure oil to pressure chamber 2 and pressure chamber 1. is connected to drain. The circuit is so designed that if the specimen breaks or there is excessive leakage in the system which leads to no pressure cycling, the machine automatically stops.

2. Hydraulic Pressure Supply.

Hydraulic pressure is supplied by a 3000 psi 3 gpm constant displacement pump driven by a 5 H.P. motor. As shown in Figure 4.3, the flow circuit contains pressure relief, throttle, bypass and flow control valves and an accumulator, oil cooler and oil reservoir. By adjusting the relief valve, discharge pressures up to 2,000 psi could be obtained. Pressures were monitored at each pressure chamber in the plate bending machine by hydraulic pressure gauges. The solenoid valve is electrically wired to allow for either automatic or manual control. An electric reset digital counter was connected in parallel to one relay. Standard SAE 30 oil was used as the hydraulic fluid.

4.4 Calibration and Measurements

Pressure-Strain measurements for each type of plate specimens were performed. The general distribution of strain in the plate specimens is of academic interest although not required for the fatigue crack propagation test program. Measurements were made at locations shown in Figure 4.8 using C12-121-A Budd strain gauges. Figure 4.9 shows the equipment used and the specimen. Readings 1 and 2 were used only for the setting of proper pressures for the tests. Figure 4.10 shows the stress profile at the longitudinal section of each series of plate specimens at test pressures used for them. Note that the major principal stress at the centre of the specimens is the same for all specimens.

4.5 Testing Procedure and Observations

The testing program is outlined in Table 4-4. The chosen range of cycles to failure was 10^4 to 10^5 cycles and the approximate stress required for the above cycles was determined by testing Series A specimens for this purpose only without taking any crack propagation readings. Now the maximum principal stress was determined which was kept constant for all the specimens.

1. Procedure for Plate Testing

The pressure switches were adjusted for correct maximum principal stress by taking readings from the strain gauge 1. A D.C. bridge amplifier meter and oscilloscope were used to obtain continuous strain readings. This way any dynamic effects and time delay of the circuit were eliminated. The counter was set at zero. The specimen was mounted in the holder with the supporting rings and pressure seals in

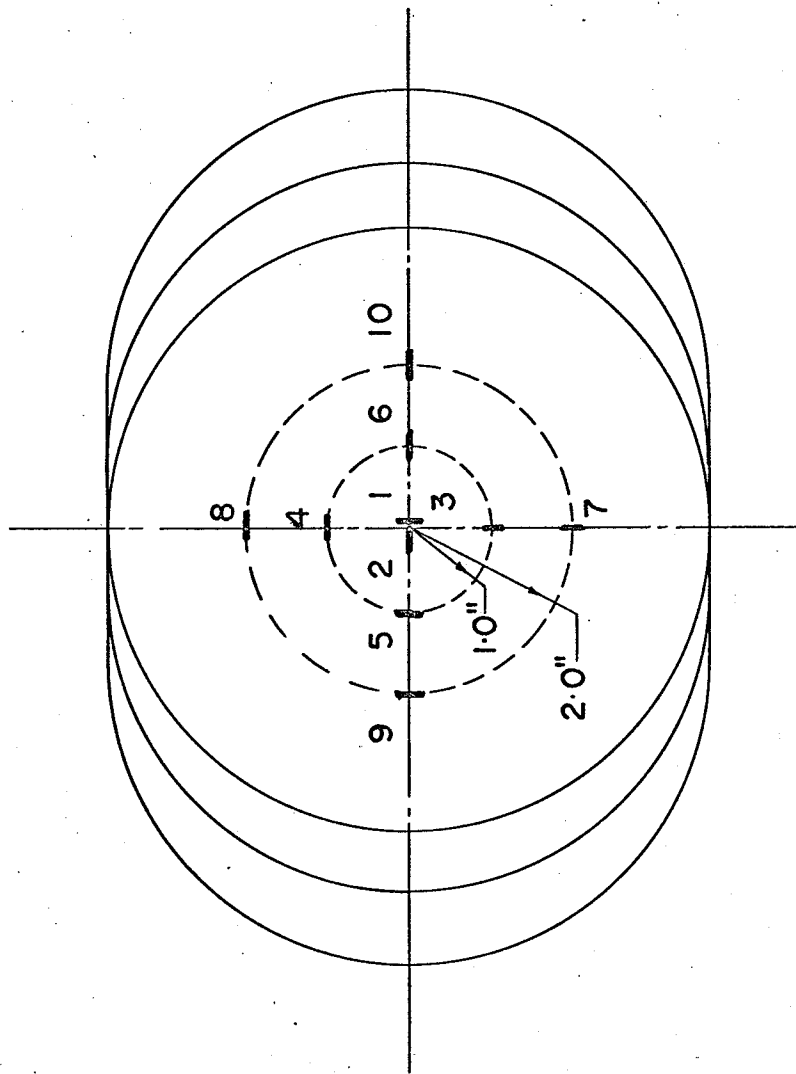


Figure 4.8 Strain Gage Location for Plate Specimens

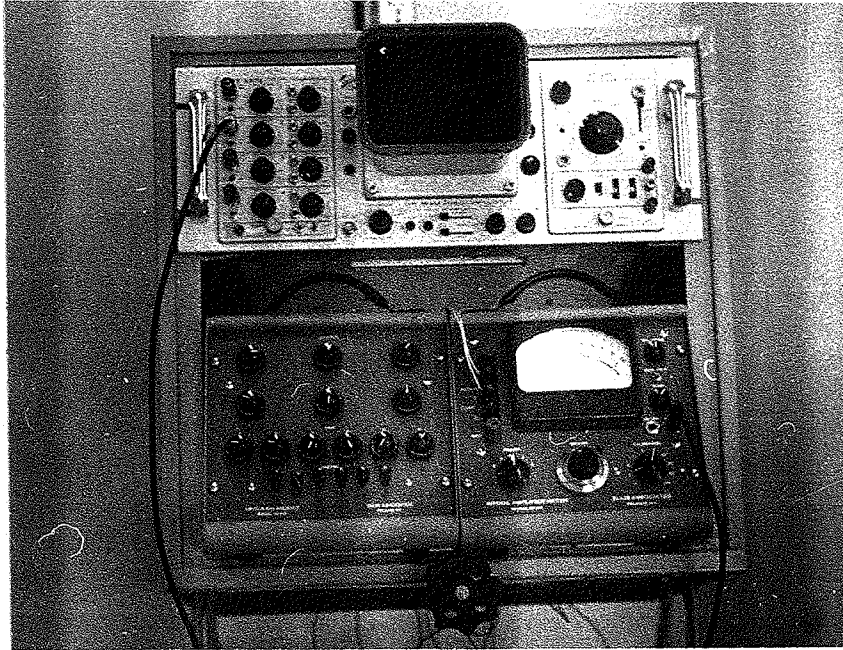


Figure 4.9A Instruments for Calibration

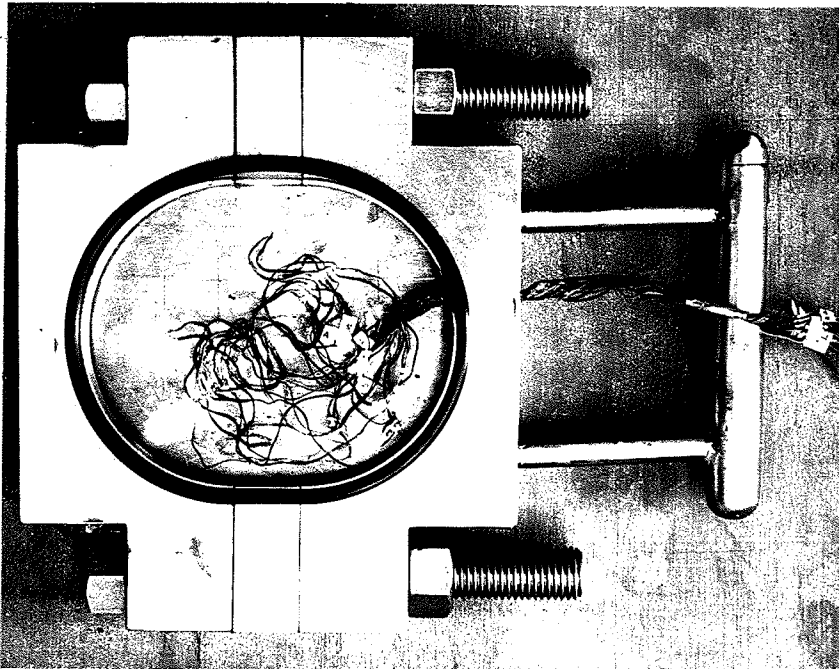


Figure 4.9B Specimen with Strain Gages

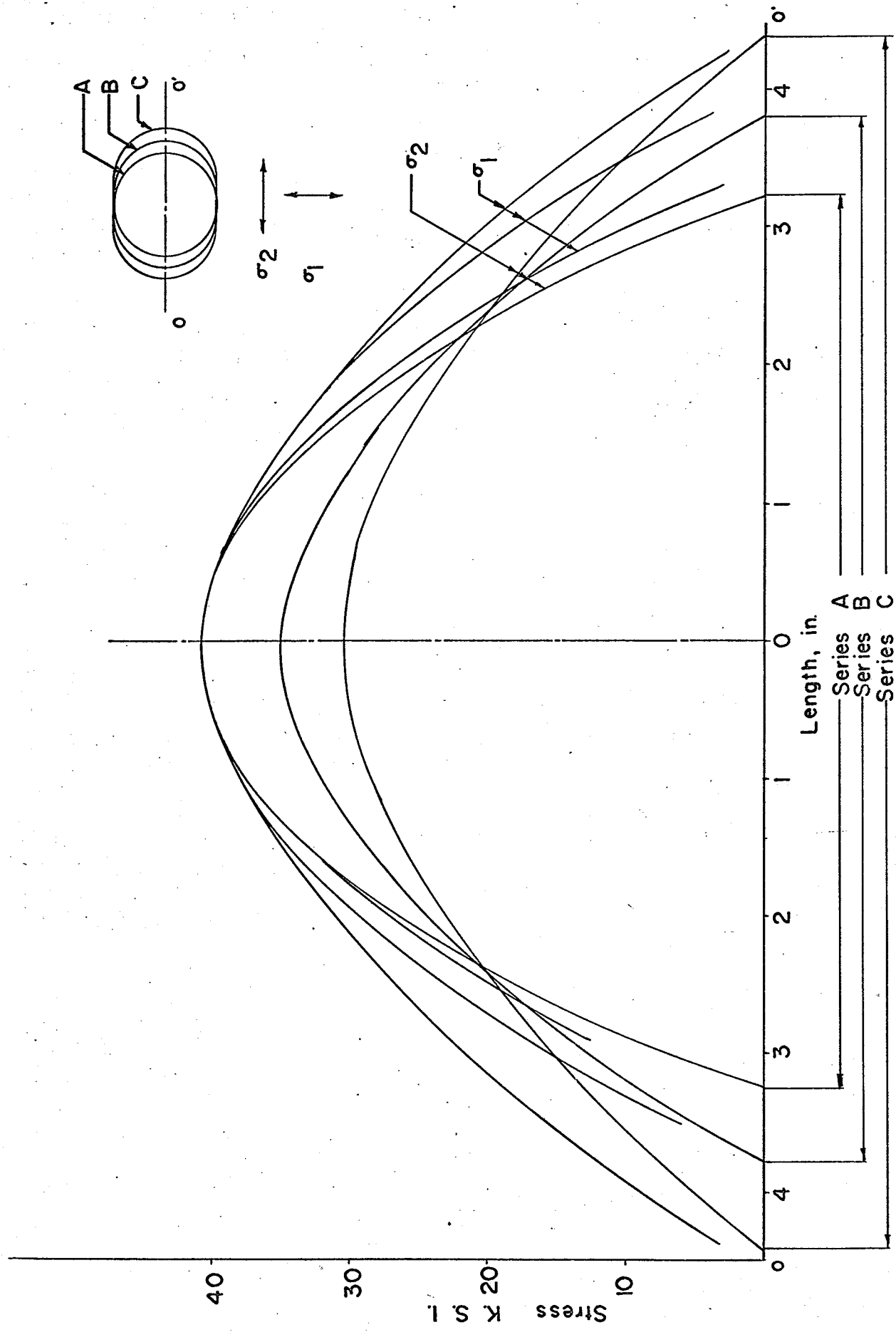


Figure 4.10 Stress Profile at Test Pressures

Table 4-4

Testing Program

Series	Minimum Principal Stress Range	Maximum Principal Stress Range
A	82,000 psi	82,000 psi
B	70,520 psi	82,000 psi
C	61,500 psi	82,000 psi

place. The holder was next slid into a central position in the pressure chamber and the eight retaining bolts were tightened.

The vent, throttle and bypass valves were opened and the solenoid energizing circuit was set for automatic operation. The pump was started and the bypass valve was partially closed causing oil to flow into the pressure chamber depending upon the position of the 4-way valve. After sufficient time was allowed for venting, the appropriate vent valve was closed and pressure started increasing until the set pressure was reached. This caused the opposing valve to be energized, thus reversing the pressure to the other side of the specimen. After the chamber was vented, the vent valve was closed and cycling now continued automatically. The bypass valve was closed and the fatigue test was in progress. The frequency of cycling was between 75 to 100 cycles per minute.

2. Observations During Plate Testing

All the specimens used had a stress raiser in the centre in the form of a notch 0.12 inch long and 0.06 inch deep. The notch was formed to force the crack to start from the centre of the specimen in the desired direction. Every 500 cycles the specimen holder was withdrawn from the pressure chamber. The crack length was measured using a microscope with X20 magnification. The crack length was measured on the side on which the notch was formed.

Failure was indicated by a stop in automatic cycling resulting from a pressure drop due to flow of oil through the specimen.

CHAPTER 5

Results and Discussion

5.1 Test Results

A total of 18 specimens was tested. Six for each series. The crack length at a different number of cycles for all specimens is given in Table 5-1, and shown graphically in Figure 5.1. In Figure 5.2 the same graph is drawn for crack length up to one inch only, as the biaxiality ratio will be nearly constant in this region. These curves are the average of six specimens tested for each series. Typical fracture patterns are shown in Figures 5.3.

5.2 Analysis of Test Results1. Introduction

The test results are compared with the theory stated in equation 3.20 to examine its validity and to determine the material constants.

2. Determination of Constants

The experimental results are again plotted in Figure 5.4. Here the rate of crack propagation is plotted against K, the stress intensity factor. Values of the rate of crack propagation at different crack lengths are obtained from Figure 5.1.

The experimental points are nearly in a straight line. The equation of the empirical curve from equation 3.20 is

$$\log_{10} \gamma = 5.6 \times 10^{-5} K - 4.27 + A_3 \frac{\tau'_{oct}}{A_4 K - \tau'_{oct}} \quad \dots 5.1$$

Here the constants in the third term are not determined as no experiments were performed to determine the endurance limit, and in any event the

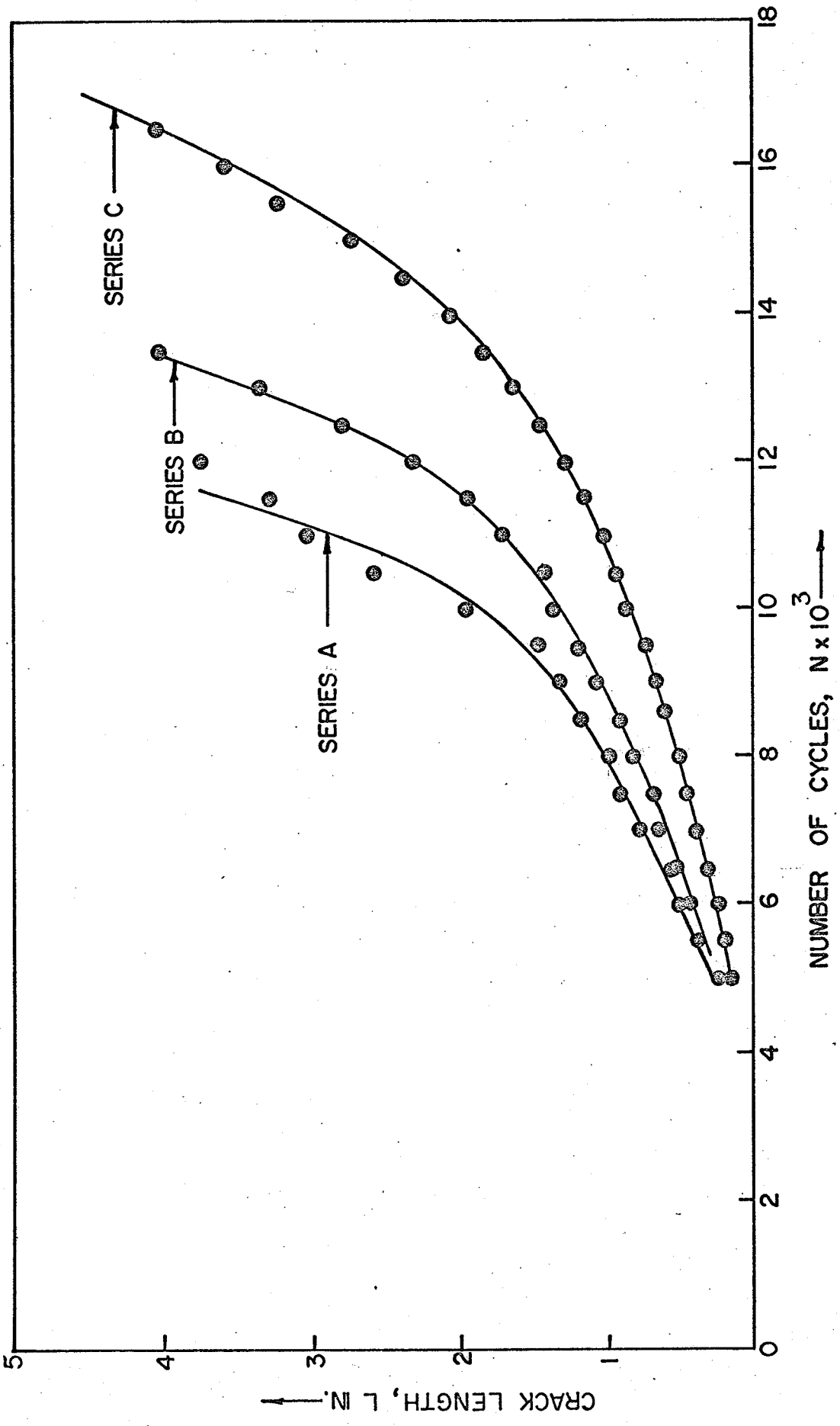


Figure 5.1 Cracks Length vs. Number of Cycles for 2024-T351 Aluminum Alloy

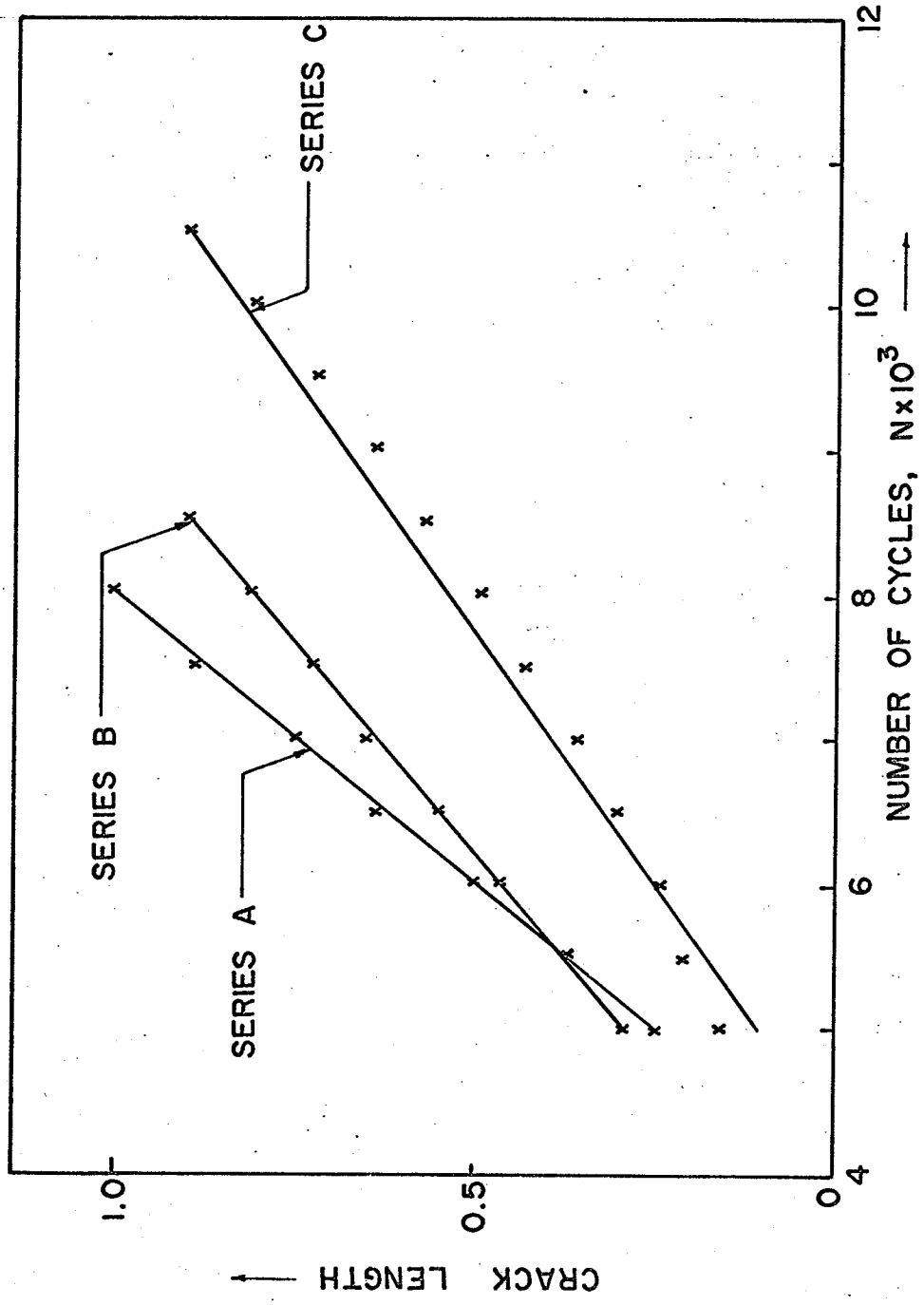


Figure 5.2 Crack Length vs. Number of Cycles for 2024-T351 Aluminum Alloy

Table 5-1A

Crack Length, l , at Different Number of Cycles for Specimens of Series A

No. of Cycles N	Crack Length, l , inches					
	1	2	3	4	5	6
5,000	0.41	0.45	0.15	0.12	0.20	0.17
5,500	0.51	0.55	0.25	0.22	0.34	0.35
6,000	0.59	0.62	0.37	0.39	0.50	0.51
6,500	0.70	0.70	0.50	0.59	0.67	0.64
7,000	----	0.78	0.65	0.83	0.78	0.78
7,500	----	0.89	0.80	1.08	0.88	0.87
8,000	0.70	1.01	0.96	1.20	1.02	1.04
8,500	0.81	1.21	1.19	1.36	1.23	1.20
9,000	0.91	1.41	----	1.51	1.44	1.39
9,500	1.00	1.59	1.30	1.67	1.62	1.60
10,000	1.09	2.38	1.52	2.41	2.38	1.83
10,500	1.19	3.61	1.78	3.08	3.72	2.11
11,000	1.40		2.10	4.10		2.51
11,500	1.69		2.80			3.10
12,000	2.42		3.87			4.01
12,500	3.41					

Table 5-1B

Crack length, l , at Different Number of Cycles for Specimens of Series B

No. of Cycles N	Crack Length, l , inches					
	1	2	3	4	5	6
5,000	0.21	0.36	0.31	0.21	0.32	0.33
5,500	0.30	0.44	----	0.30	----	0.40
6,000	0.38	0.50	0.50	0.39	0.50	0.49
6,500	0.47	0.58	----	0.46	----	----
7,000	0.58	0.66	0.69	0.58	0.70	0.68
7,500	0.65	0.74	----	0.65	----	0.77
8,000	0.73	0.86	0.85	0.74	0.82	0.87
8,500	0.86	0.94	0.92	0.85	0.92	0.91
9,000	0.96	1.16	1.06	0.99	1.06	1.09
9,500	1.10	1.26	1.19	1.10	1.20	1.20
10,000	1.27	1.40	1.37	1.37	1.38	1.37
10,500	1.52	1.57	1.46	1.42	1.42	1.53
11,000	1.63	1.80	1.62	1.67	1.67	1.71
11,500	1.95	2.15	1.81	1.90	1.82	1.95
12,000	2.30	2.60	2.19	2.34	2.16	2.30
12,500	2.82	3.15	2.65	2.83	2.51	2.78
13,000	3.32	3.90	3.21	3.42	2.90	3.30
13,500	4.20		3.90		3.32	3.90
14,000			4.90		3.80	4.70
14,500					4.40	

Table 5-1C

Crack Length, l , at Different Number of Cycles for Specimens of Series C

No. of Cycles N	Crack Length, l , inches					
	1	2	3	4	5	6
5,000	0.12	0.14	0.14	0.23	0.12	0.19
5,500	----	----	0.18	0.30	0.12	0.24
6,000	0.21	0.27	0.23	0.34	0.12	0.29
6,500	----	----	0.30	0.39	0.20	0.34
7,000	0.33	0.33	0.39	0.42	0.28	0.40
7,500	0.41	0.40	0.49	0.47	0.35	0.47
8,000	0.51	0.47	0.51	0.52	0.42	0.51
8,500	0.57	0.53	0.58	0.53	0.58	0.62
9,000	0.64	0.62	0.64	0.63	0.62	0.70
9,500	0.72	0.70	----	----	0.71	0.80
10,000	0.82	0.78	0.76	0.76	0.82	0.90
10,500	0.93	0.90	----	----	0.91	1.02
11,000	1.04	0.98	0.92	0.94	1.06	1.15
11,500	1.19	1.09	1.01	1.04	1.18	1.30
12,000	1.33	1.20	1.10	1.14	1.31	1.49
12,500	1.56	1.32	1.21	1.26	1.48	1.72
13,000	1.80	1.49	1.33	1.40	1.63	2.04
13,500	2.09	1.67	1.46	1.51	1.82	2.39
14,000	2.40	1.84	1.60	1.68	2.10	2.80
14,500	2.81	2.07	1.78	1.84	2.39	3.38
15,000	3.21	2.39	2.01	2.02	2.74	4.01

Table 5-1C (Continued)

No. of Cycles N	Crack Length, l , inches					
	1	2	3	4	5	6
15,500	3.68	2.80	2.31	2.29	3.19	
16,000	4.23	3.30	2.70	2.60	3.61	
16,500		3.92	3.15	2.96	4.15	
17,000			3.68	3.35		
17,500			4.29	3.90		
18,000				4.41		

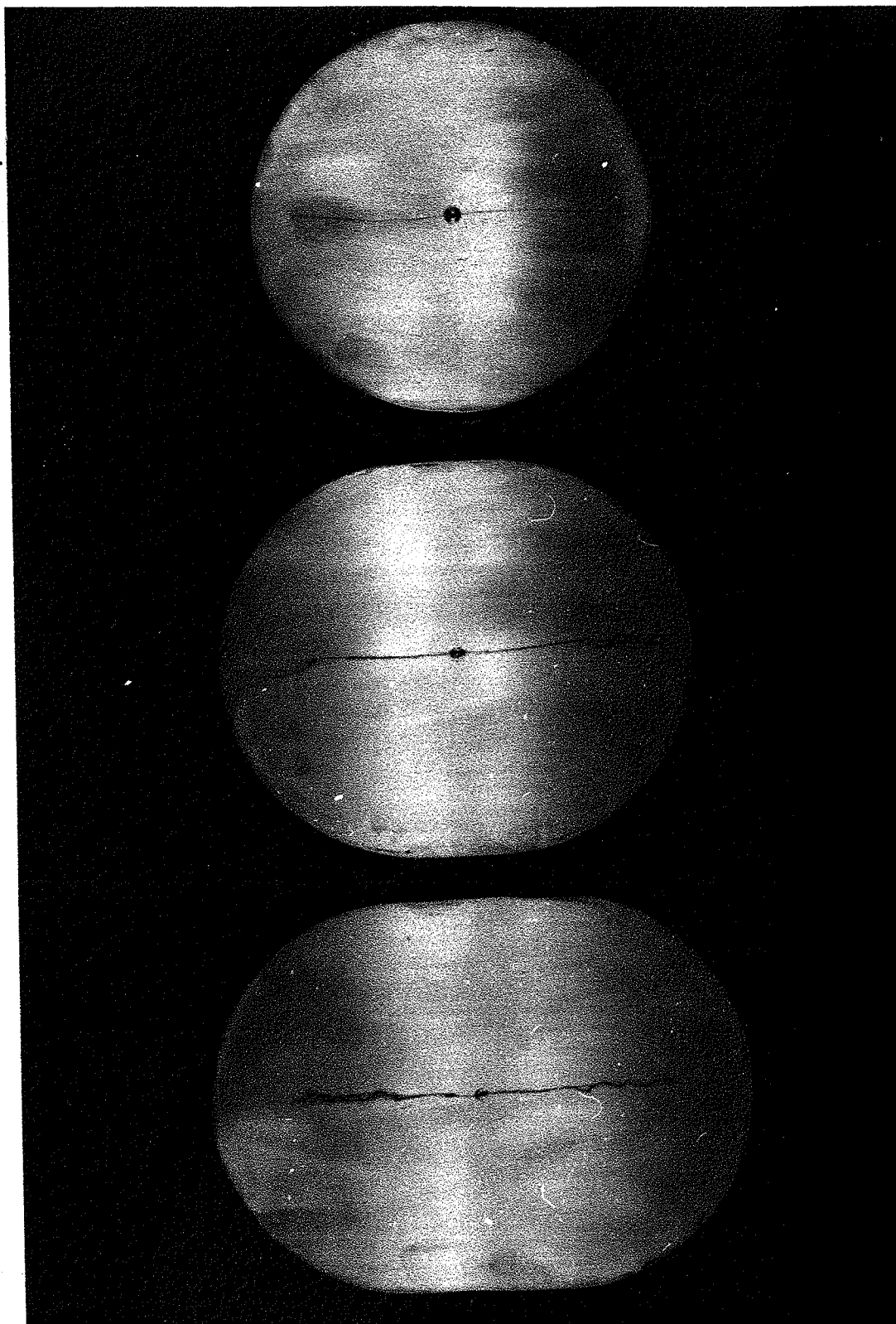


Figure 5.3 Typical Fracture Patterns

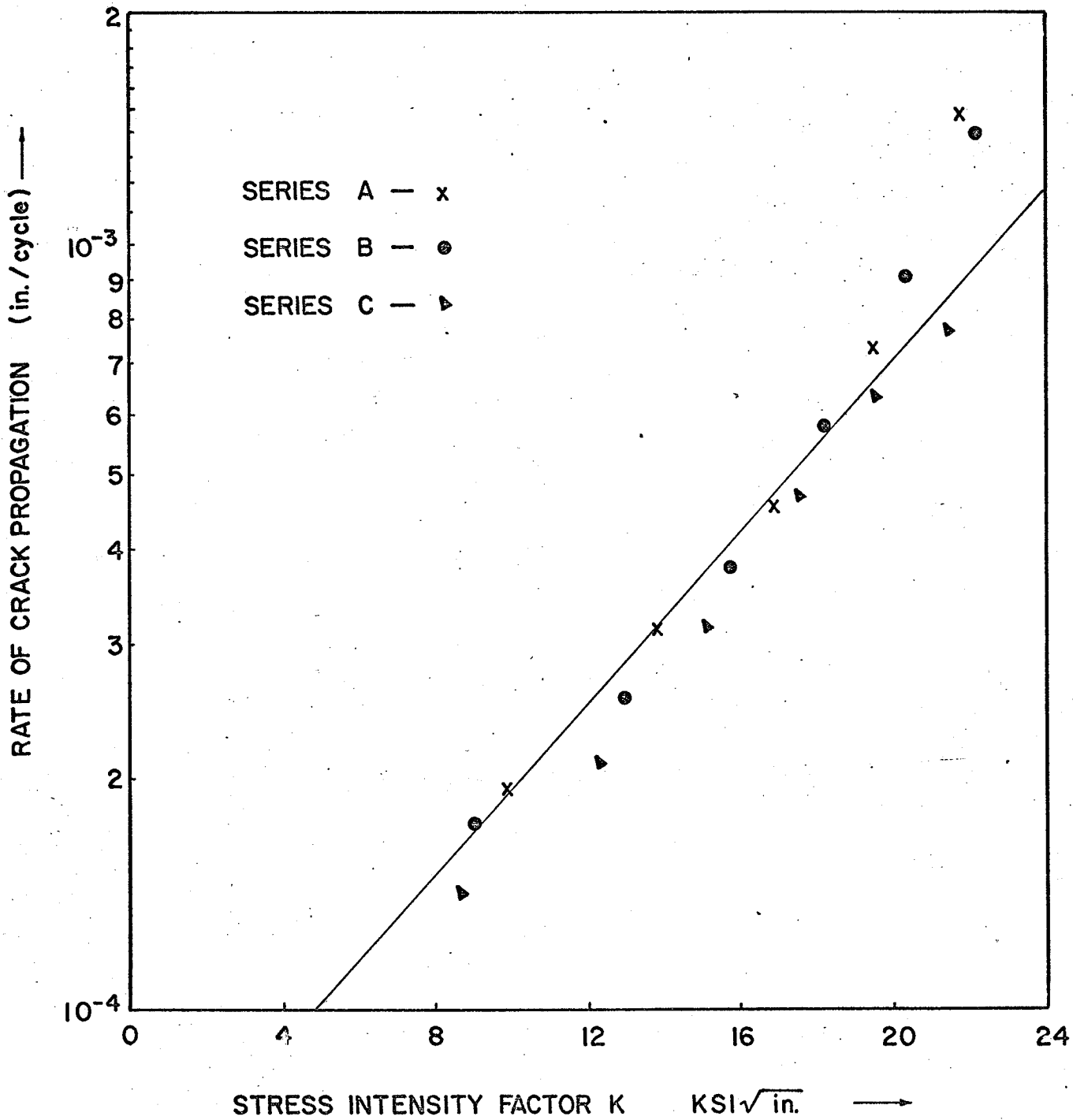


Figure 5.4 Rate of Crack Propagation vs. Stress Intensity Factor for 2024-T351 Aluminum Alloy

third term has negligible effect on the rate of crack propagation at the stress levels used for the experiments.

5.3 Discussion

In the proposed empirical biaxial fatigue crack propagation equation, 3.20, it can be observed that "r" the rate of crack propagation depends upon K and τ'_{oct} . The third term ($A_3 \tau'_{oct} / A_4 K - \tau'_{oct}$) should tend to minus infinity as the octahedral stress approaches the endurance limit.

To obtain some idea of the two constants, A_3 and A_4 , the empirical curve is extrapolated in Figure 5.5. From survey of available literature the uniaxial endurance limit for 2024-T3 aluminum alloy in axial load tests is 20,000 psi (Reference (28)). Assuming a load factor of 0.8 for bending tests, the endurance limit in uniaxial bending is 25,000 psi.

Therefore

$$\tau'_{oct} = \frac{\sqrt{2}}{3} S_f = 11.8 \text{ ksi.} \quad \dots 5.2$$

For the third term to tend to infinity the denominator should be zero at the endurance limit.

$$A_4 K - \tau'_{oct} = 0 \quad \dots 5.3$$

$$A_4 = 12.9 \quad \dots 5.4$$

For the rate of crack propagation to tend to zero the constant A_3 should have a negative value. $A_3 = -0.168$ gives the best fit for the extrapolated curve.

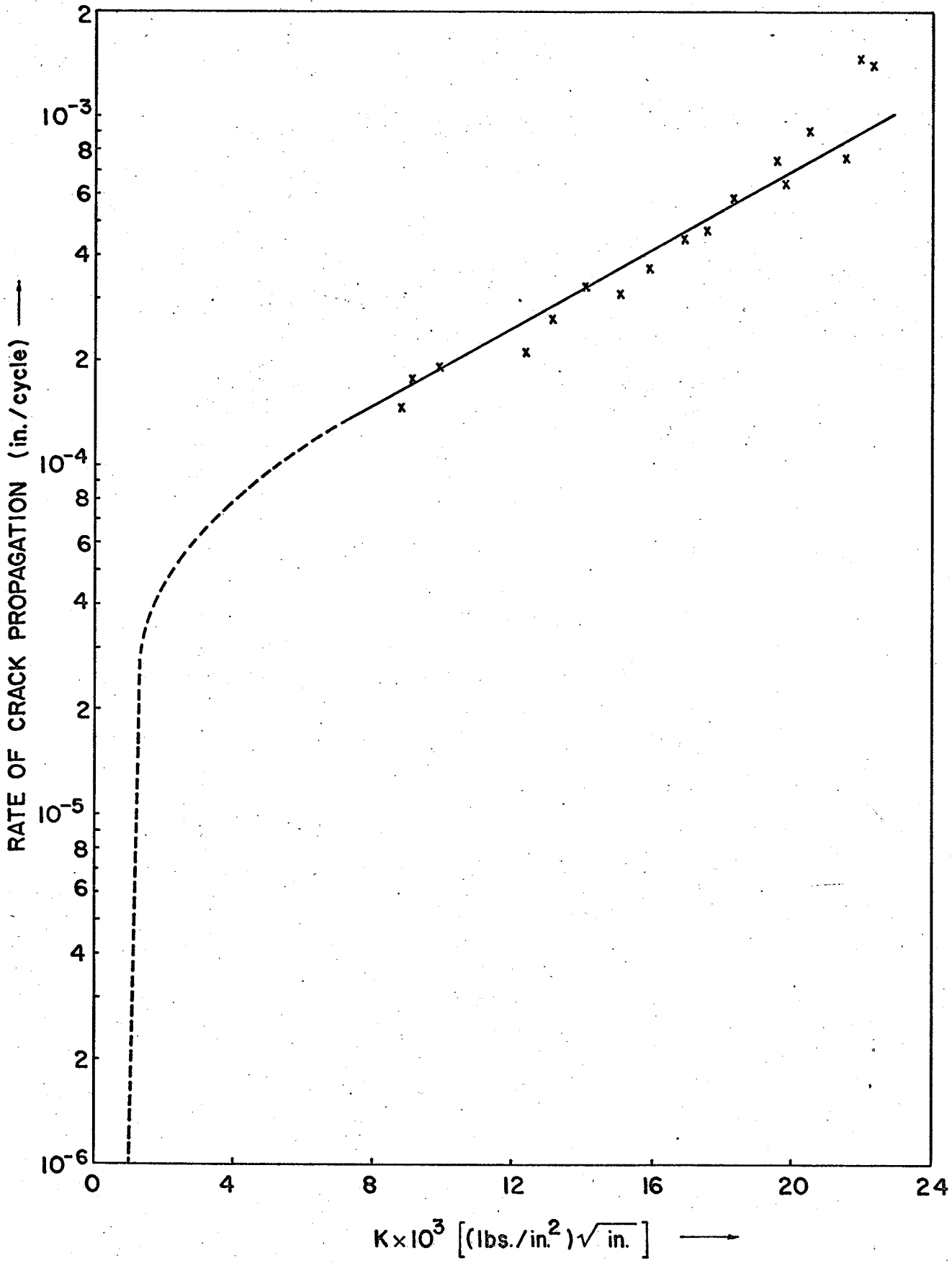


Figure 5.5 Rate of Crack Propagation vs. Stress Intensity Factor for 2024-T351 Aluminum Alloy

The stress intensity factor K is

$$K = \tau'_{\text{oct}} a^{1/2} \quad \dots 5.5$$

The use of this factor to predict the rate of crack propagation is very useful as all data can be converted and plotted on the same graph.

$$\tau'_{\text{oct}} = \frac{1}{3} \sqrt{(\sigma_1 - \sigma_2)^2 + (\sigma_2 - \sigma_3)^2 + (\sigma_3 - \sigma_1)^2} \quad \dots 5.6$$

For uniaxial test $\sigma_2 = \sigma_3 = 0$

$$\tau'_{\text{oct}} = \frac{\sqrt{2}}{3} \sigma_1 \quad \dots 5.7$$

For biaxial test $\sigma_3 = 0$

$$\tau'_{\text{oct}} = \frac{\sqrt{2}}{3} \sqrt{\sigma_1^2 + \sigma_2^2 - \sigma_1 \sigma_2} \quad \dots 5.8$$

If we maintain σ_1 constant and vary σ_2 , the lowest value of τ'_{oct} is obtained for

$$\sigma_2 = 0.5 \sigma_1 \quad \dots 5.9$$

For the experiments performed σ_1 was kept constant, and σ_2 was changed, the values of σ_1 and σ_2 used for different series of specimens is given in Table 4-4.

The Figure 5.1 clearly indicates that the minor stress σ_2 has an effect on the rate of crack propagation. For all the three series the major stress $\sigma_1 = 41,000$ psi was kept constant and only σ_2 was changed. It can be concluded that the octahedral shear stress is a better indicator of the stress amplitude than maximum stress for biaxial fatigue crack propagation.

CHAPTER 6

Summary and Conclusion

6.1 Summary

The effect of biaxiality of stress on the rate of fatigue crack propagation has been studied in this thesis.

High cycle biaxial fatigue crack propagation characteristics of 2024-T351 aluminum alloy plate were investigated. A machine was designed and constructed for reversed bulging of round and elliptical plates with different ratios of surface principal stresses. The stress ratios investigated were 1.0, 0.86 and 0.75. For all the stress ratios investigated specimens were used with transverse orientation of maximum principal stress axis with respect to the rolling direction of the material.

A theory is presented to predict the rate of fatigue crack propagation for biaxiality ratios between 0.5 and 1.0.

6.2 Conclusion

Supported by the test data obtained from the experiments described in this thesis and by data obtained in a literature survey as acknowledged by reference the following conclusions are made:

1. The equipment designed and constructed for the experimental portion of this thesis is quite satisfactory for investigation of high cycle fatigue in bending with varying degree of biaxiality stress. The maximum speed of the machine is 18,000 cycles per hour, this limits the use of the machine for very high cycle fatigue experiments from time considerations.

2. The biaxiality of stress does have an effect on the rate of fatigue crack propagation. For biaxiality ratios between 0.5 and 1.0, it is observed that the rate of crack propagation increases as the biaxiality ratio increases.

6.3 Suggestion for Further Study

For further understanding of the effects of biaxiality on the rate of fatigue cracks propagation tests should be done for biaxiality ratios below 0.5.

BIBLIOGRAPHY

- (1) Moore, H.F., University of Illinois Engineering Experimentation Station, Bullitine No. 165, 1927.
- (2) Forest, A.V., "The Rate of Growth of Fatigue Cracks", Trans. ASME, Vol. 58, 1936, p. A-23.
- (3) Head, A.K., "The Growth of Fatigue Cracks", Philosophical Magazine, Sec. 7, Vol. 44, No. 356, Sept. 1953, p. 925.
- (4) Head, A.K., "The Propagation of Fatigue Cracks", ASME Trans.-D, Vol. 78, 1956, p. 407.
- (5) Campbell Laird, "The Influence of Metallurgical Structure on the Mechanism of Fatigue Crack Propagation", Fatigue Crack Propagation, ASTM STP 415, Am. Soc. Testing Mats., 1967, p. 131.
- (6) Laird, C., and Smith, G.C., "Initial Stages of Damage in High Stress Fatigue", Philosophical Magazine, Vol. 8, 1963, p. 1945.
- (7) Christensen, R.H., and Harmon, M.B., "Limitations of Fatigue Crack Research in the Design of Flight Vehicle Structures", Fatigue Crack Propagation, ASTM STP 415, 1967, p. 5.
- (8) Whaley, R.E., and McGuigan, M.J., "Fatigue Crack Propagation and Residual Static Strength Results on Full Scale Transport Airplane Wings", NACA Technical Note 3847, December, 1956.
- (9) Hudson, C.M., and Hardrath, H.F., "Effects of Changing Stress

Amplitude on the Rate of Fatigue Crack Propagation in two Aluminum Alloys", NACA Technical Note D-960, Sept. 1961.

- (10) Jacoby, G., "Application of Microfractography to the Study of Crack Propagation under Fatigue Stresses", North Atlantic Treaty Organization, AGARD Report 541, 1966.
- (11) Laird, C., and Smith, G.C., "Crack Propagation in High Stress Fatigue", Philosophical Magazine, Vol. 7, 1962, p.847.
- (12) Paris, P., and Erdogan, F., "A Critical Analysis of Crack Propagation Laws", ASME Trans.-D, Vol. 85, 1963, p.528.
- (13) Cotterell, B., "An Interpretation of the Mechanics of Crack Growth by Fatigue", ASME Trans.-D, Vol. 87, 1965, p.230.
- (14) Irwin, G.R., "An Analysis of Stress and Strain Near the End of the Crack Traversing a Plate", ASME Trans.-D, Vol. 79, 1957, p. 361.
- (15) Jäcoby, G., "Fractographic Methods in Fatigue Research", Experimental Mechanics, 1965, p. 65.
- (16) Liu, H.W., "Crack Propagation in Thin Metal Sheets Under Repeated Loading", ASME Trans.-D, Vol. 83, 1961, p. 23.
- (17) Liu, H.W., "Fatigue Crack Propagation and Applied Stress Range - An Energy Approach", ASME Trans.-D, Vol. 85, 1963, p.116.
- (18) Eftis, J., and Krafft, J.M., "A Comparison of the Initiation with Rapid Propagation of a Crack in Mild Steel Plate", ASME Trans.-D, Vol. 87, 1965, p. 257.

- (19) Frost, N.E., and Dugdale, D.S., "The Propagation of Fatigue Cracks in Sheet Specimens", *Journal of Mechanics and Physics of Solids*, Vol. 6, No. 2, 1958, p. 92.
- (20) McEvily, A.J., and Illg, W., "The Rate of Fatigue Crack Propagation in Two Aluminum Alloys", NACA Technical Note 4394, 1958.
- (21) Illg, W., and McEvily, A.J., "The Rate of Fatigue Crack Propagation for Two Aluminum Alloys Under Completely Reversed Loads", NACA Technical Note D-52, October 1959.
- (22) Orowan, E., "Theory of the Fatigue of Metals", *Proc. Roy. Soc. (London)*, Ser. A. Vol. 171, No. 944, 1939, p. 79.
- (23) Wood, W.A., and Segall, R.L., "Annealed Metals Under Alternating Plastic Strain", *Proc. Roy. Soc. (London)*, Ser. A, Vol. 242, No. 1229, 1957, p. 180.
- (24) Huber, M.T., *Czasopismo Techniczne, Lwów (Lemberg)*, 1904.
- (25) Timoshenko, S., *Strength of Materials - Part II - Advanced Theory and Problems*, 3rd ed., D. Van Nostrand Company Inc., Princeton, New Jersey, 1956, p. 455.
- (26) Irwin, G.R., "Fracture Mode Transition for a Crack Traversing a Plate", *ASME Trans.-D*, Vol. 82, 1960, p. 417.
- (27) Shewchuk, J., Zamrik, S.Y., and Martin, J., "Low-Cycle Fatigue of 7075-T651 Aluminum Alloy in Biaxial Bending", *Experimental Mechanics*, November, 1968, p. 504.

- (28) Majors, H., Mills, B.D., and MacGregor, C.W., "Fatigue Under Combined Pulsating Stress", Journal of Applied Mechanics, Vol. 15, September 1949, p. 269.
- (29) Paris, P.C., "A Note on the Variables Affecting the Rate of Crack Growth Due to Cyclic Loading", Boeing Company Document, No.-D-17867, Addendum N, September 12, 1957.